NANYANG
TECHNOLOGICAL
UNIVERSITY

SELECTIVE LASER MELTING OF CERAMIC-BASED MATERIALS FOR DENTAL APPLICATIONS

NAVITA MAPAR

SCHOOL OF MECHANICAL AND AEROSPACE ENGINEERING

2014

Selective Laser Melting of ceramic-based materials for dental applications

Mahta Mapar

School of Mechanical and Aerospace Engineering (MAE)

A thesis submitted to the Nanyang Technological University

In partial fulfillment of the requirement for the degree of

Master of engineering

2014

Abstract

The employment of the Selective Laser Melting (SLM) technique in the processing of ceramics has attracted attention recently. SLM is a powder-based AM process where powder spreading is one of the fundamental. Therefore, a spray-drying process was chosen to improve powder properties to reach a proper powder for the SLM process. Also a dynamic powder characterisation methodology was used to investigate powder flow characteristic.

A series of SLM experiments were conducted using the spray-dried powder in three stages: single-track melting, single-layer melting and fabrication of three-dimensional (3D) blocks (multilayers). The objectives of this set of experiments were to establish the preliminary processing windows of ceramics via SLM.

Finally, multilayer or ceramic 3D blocks were experimented via SLM machine. However, the density of the fabricated 3D parts was low and the parts were also fragile and unstable. These results showed that with current state of technology, it is still a challenge to directly fabricate dense ceramic components using SLM. Following the insights obtained from these experiments, the critical challenges of this project were identified and discussed, including ceramic powder layer deposition, laser-powder particles interaction, the dynamic melting and consolidation mechanism, process parameter optimisation and residual stress analysis of the ceramic materials processed with SLM.

Keywords: Selective Laser Melting, ceramic, powder flow, Revolution Powder Analyzer, 3D blocks.

Acknowledgements

I would like to express my deepest appreciation to Assistant Professor Yeong Wai Yee and Dr Tay Bee Yen for their patience, support and continual guidance during the course of this research. They have been very approachable and often provided feedback and academic advice that enabled the smooth running of the research.

My gratitude also goes to the researchers and executives in SIMTech-NTU Joint Laboratory on 3D Additive Manufacturing at NTU for lending their support in the project in terms of facilities and expertise.

I am grateful for the scholarship by *Agency for Science Technology & Research (A*STAR)*. Also I am thankful to NAMC and SIMTech for providing all facilities and materials for this project.

Lastly, thanks to my dear husband, Zia, for his continued and unfailing love, support and understanding underpins my persistence in the graduate career and makes the completion of this thesis possible.

I dedicate this thesis to my family and my husband for their constant support and unconditional love.

Table of contents

List of tables

List of figures

List of Abbreviations

AM	Additive Manufacturing
CAD	Computer Aided Design
EDXS	Energy Dispersive X-ray Spectroscopy
FDM	Fused Deposition Modeling
FESEM	Field Emission Scanning Electron Microscopy
LOM	Laminated Object Manufacturing
MAE	School of Mechanical and Aerospace Engineering
NAMC	NTU Additive Manufacturing Center
Nd:YAG	Neodymium doped Yttrium Aluminium Garnet
NTU	Nanyang Technological University
RP	Rapid Prototyping
SEM	Scanning Electron Microscopy
SIMTech	Singapore Institute of Manufacturing Technology
SLM	Selective Laser Melting
SLS	Selective Laser Sintering
TCP	Tri-Calcium Phosphate
TEM	Transmission Electron Microscopy
XRD	X-Ray Diffraction
YSZ	Yttria-stabilized Zirconia
3D	3-Dimensional
3DP	Three-Dimensional Printing

Chapter 1: Introduction

1.1 Background

Additive manufacturing (AM) processes allow the production of components by adding materials, in contrast to subtractive manufacturing such as machining processes. Selective laser melting (SLM) is an AM process which is able to produce three-dimensional (3D) complex shapes. During the process each layer of powder materials is selectively melted according to computer-aided design (CAD) data. The needed energy for the melting is produced by laser radiation [1].

One of the advantages of SLM in comparison with conventional methods is its capability to manufacture complex geometries in a wide spectrum, such as internal structures and intricate geometry elements which are not realisable with other processes, even the investment casting process. Final parts are built layer by layer according to the cross-section area of products in CAD data. There is no need for post-processes such as milling and grinding. This allows the manufacturing of individual pieces and small numbers of components in a cost effective and fast manner.

SLM as a rapid manufacturing method for metallic materials has already been adopted in industry. However, for ceramic material no comparable procedure exists. Currently, available AM processes for ceramic materials are based on sintering treatment, which is not able to produce fully dense components.

Therefore, the aim of this project is to explore the use of the SLM method for ceramic materials.

This research focuses on a mixture material of zirconia (ZrO_2) and alumina (Al_2O_3). Both ZrO_2 and Al_2O_3 are two important structural ceramics from the group of oxide ceramics, which because of their mechanical properties are ideal for both technical and medical applications. Non-oxide ceramics such as silicon nitride are not suitable for the SLM process because they decompose at high temperatures before even forming a melt phase. The targeted application for developing the process is the production of individual ceramic restoration for dental applications. The key point of using the SLM method for this aim is to produce individualised ceramic parts quickly and inexpensively. Demand for such products in the marketplace is huge and continues to grow because of the benefits of the improved aesthetics and biocompatibility of ceramic restorations compared with metallic ones. Other possible applications are the production of a functional prototype in the technical area and application as a rapid manufacturing method for complex geometric components that cannot be produced through other methods or that cannot be produced in an economically feasible way.

1.2 Motivation:

Compared with the conventional production methods of ceramics, AM, in particular SLM has two advantages. One is its ability to support large-geometric freedom, an important issue for ceramics when creating intricate parts. As there are fewer available moulding processes for ceramics than metal materials, geometric freedom in ceramics is more critical. For example, casting is not capable of manufacturing complex geometries. Other metal forming manufacturing processes such as forging, drawing, etc. are unable to process ceramic materials due to their brittle properties. Cutting a green shape, i.e. so-called "green machining", is only possible for slightly sintered powder bodies. The conventional shaping process for ceramics, such as the sintering process, has its limitations due to shrinkage and crack formation, which cause geometric inaccuracies. Furthermore, manufacturing complex shapes with conventional methods is time consuming and costly due to the steps which are needed for construction, assembly, and post-processing. SLM can solve this problem with direct production in one-step. In the SLM process, no tools are required for specific shapes and geometries. Moreover, SLM is more cost effective than other manufacturing processes when it comes to producing small quantities of customised products.

The basic application of using SLM to produce ceramic parts is for dental restorations such as frameworks for crowns or bridges. The frameworks which are currently used in dental laboratories are metallic materials coated with a veneer to improve their aesthetics. Thus, the framework is a support structure for the dental restoration, which is fit to the patient specifics. Producing a full ceramic dental

restoration in comparison to restoration with a metal framework has the advantages of better aesthetics and biocompatibility. Therefore, there is an increasing demand for all-ceramic restorations in the marketplace. Currently all-ceramic restorations are made of ZrO_2 due to its high strength. A widely used method for ZrO_2 production is grinding or milling of sintered ceramic bulks integrated with a CAD/computer-aided manufacturing (CAM) process. Due to this, there is the possibility of producing all-ceramic restorations with SLM technology at a lower price than the other alternative methods. Unlike machining processes, tool wear is not a challenge in SLM and the process is capable of producing large numbers of customised restorations (for example 70 parts) at once.

Al_2O_3 and ZrO_2 are two ceramics whose privileged properties, including high strength, corrosion resistance, and wear resistance, make them the ideal candidates for dental restorations. So far, no rapid manufacturing process has been recognised as capable of successfully producing high density, highly resistant, and dimensionally accurate ceramic parts with ZrO_2 and Al_2O_3. The numerous attempts that have been made so far have limitations such as porosity, lack of shape accuracy, or low strength of the final part. In addition, these methods require a sintering treatment that is always accompanied by shrinkage, which can affect the part's geometric accuracy. Therefore, these problems create an incentive to fabricate ceramics dental implants from ZrO_2 and Al_2O_3 with high density, high resistance, and good dimensional accuracy using SLM.

1.3 Objective

The objectives of this research are as follows:

1. To assess the capability of an SLM machine in processing ceramic materials directly.
2. To determine the optimal process parameters for the fabrication of ceramic parts using SLM.

Using this laser-based generative manufacturing process has the potential to produce full dense ceramic parts without sintering treatment. High-strength parts with near full density are required for dental restorations. As SLM is more cost-effective than established methods in the market, there is a high demand for ceramic parts built with SLM in the same way metals are.

1.4 Scope

The scope of this project includes:

1. Preparing a suitable powdered material as the raw material for SLM.
2. Performing a series of experiments, including single-track and single-layer melting, to determine the optimal process parameters for building ceramic parts with SLM.
3. Fabricating 3D blocks of ceramic with the SLM process
4. Investigating the properties of fabricated parts through material characterisation tests, such as X-ray diffraction (XRD), scanning electron microscopy (SEM), and density tests based on Archimedes' principles.

1.5 Organisation of the report

This report begins with the introduction chapter describing the baclkground, motivation, objectives, and scope of this research project.

Chapter 2 covers the literature review, comparing different conventional manufacturing methods with AM methods for ceramic materials, and an extensive review of the materials used in SLM together with their applications. The properties of ZrO_2 and Al_2O_3 as the two selected ceramic materials in this research are also provided. Chapter 3 illustrates the procedures of the experiments on ceramic materials, including powder preparation and SLM processing, and the results of the experiments are discussed in Chapter 4. Chapter 5 presents the conclusions of the study and possible future work as well as the publications resulting from the current work.

Chapter 2: Literature review

2.1 Forming processes of ceramics

2.1.1 Conventional manufacturing methods of ceramics

The starting point for manufacturing objects made of ceramic materials is powder. Most of the conventional methods include steps of powder production, shaping, and sintering [2] and, if necessary, continued shaping treatment after sintering.

Shaping methods which are suitable for complex shapes are as follows:

1) Slipcasting

Slipcasting is the process of producing ceramic forms by pouring a slip into a plaster mould to solidify. The main consolidation process is the compaction of the ceramic powder particles on the mould wall. This method is widely used for hollow part production, but in other cases a full cast method is also possible [3].

The advantage of slipcasting is the possibility of large volume production of complexly shaped components. In the other hand, production of single pieces or small numbers of parts is a form of disadvantage for this method.

2) Injection moulding

Complex technical ceramic parts are commonly formed using either the injection moulding process or "hot wax moulding". This method relies on adding thermoplastic materials to ceramic powders to allow material flow into a metal die. The part is then quickly cooled for ejection from the mould. The thermoplastic binder must be removed before sintering treatment [4].

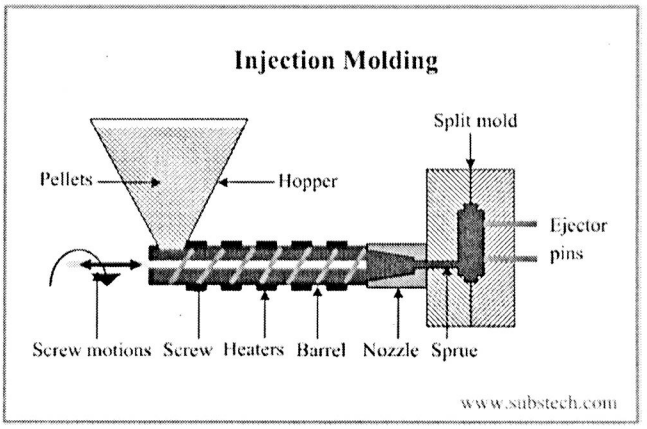

Figure 1 Injection moulding process

Ceramic injection moulding is much like plastic injection moulding, using various polymers for plasticising. This method can be used for the mass production of small, complex parts. However, a new mould is needed for the production of each of the customised geometries. Therefore, this method is not economically viable for single pieces or small production numbers.

3) Green and white machining

Green machining is performed on a green body. A green body is a shaped solid that has not yet been fired and that contains organic additives which bind the whole body together. As a green body has low strength compared with a fired body, this method is suited to the manufacture of shapes that cannot be realised directly by the initial forming procedure, such as holes transverse to the direction of the dry pressing. The manufacturing process includes cutting, stamping, drilling, turning, sawing, and grinding [5].

White machining is referred to as preliminary firing, which is performed on prefired parts. The prefired parts are free from organic additives and their strength depends on the prefiring. In this way, extremely high removal rates can be achieved

with relatively low tool wear using conventional, ceramic-coated, or diamond-coated tools. This process is used by manufacturers to perform ceramic restoration, which is also known as the last step of shape modification in hard machining processes. Furthermore, this process is able to produce a near net shape for final parts. The fabricated parts achieved only 3% relative dimensional tolerance in normal procedures. Even precision processes may achieve 1% relative dimensional tolerance[6]. The disadvantage of this method is high tool wear, which is an associated cost. Lacking the ability for net shape fabrication, low dimensional tolerance, and the high cost for special blanks are major drawbacks to the dental applications of this method.

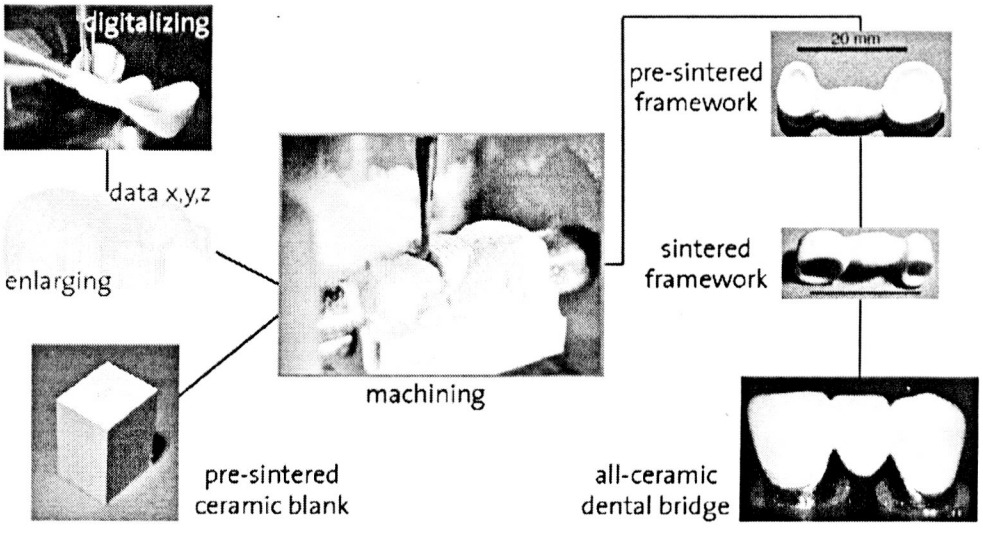

Figure 2 Machining process of technical components [6].

4) Processing in a sintered state

Even after a part has undergone sintering treatment to make it dense, a shaping process can still be used. However this is usually limited to grinding with tools based on diamond, boron, and silicon carbide, which is called hard machining. Hard machining systems use abrasives for micro removal of particles from a dense sintered part [7]. This method produces very accurate parts with a good surface finish. However, hard machining processes are slow and need special tools and cooling media, which make them very expensive.

2.1.2 Additive manufacturing (AM) process for ceramic materials

An additive process is a procedure in which the geometry of a component is formed by adding materials without using a master mould. In most cases material is added layer by layer in AM, in contrast to subtractive manufacturing methodologies. The following AM processes have already been tested for ceramic materials:

- 3D printing (3DP)
- Ink-jet printing
- Fused deposition modelling (FDM)
- Laminated object manufacturing (LOM)
- Laser-based methods (stereolithography, selective laser sintering)

In the following section, these methods are briefly introduced and the current state of the art is described. In this case, works that deal with oxide ceramics in particular are included. Methods which are used for other ceramics such as SiC, Si3N4, etc. are not treated in detail because the chosen materials for this study are oxide ceramics.

1) 3DP

This is the classic 3DP powder-based method. 3DP is achieved using an additive process, where successive layers of material are laid down on the build platform. After this a print head selectively introduces a binder in the desired areas of the powder layer and the powder is solidified. Sachs *et al.* used this method for Al_2O_3 powder combined with a binder and silica (SiO_2) nanopowder dispersed into a liquid [8]. The complete 3D part is then heated up in a furnace to remove the binder and sinter the green body. Residual porosity in the final parts and restriction of the material combination are disadvantages of this process. The combination of Al_2O_3 and SiO_2 in this case does not reach the required strength of 500 MPa for dental restoration.

2) Slurry-based 3DP (S-3DP)

The difference between classic 3DP and S-3DP is the method of sequential layer deposition during the process. Each layer is formed in S-3DP by slipcasting a slurry of ceramic powder onto a porous structure. Following this, a drying step removes solvent/dispersing materials. Binder is then printed in the same method as classic 3DP using ink-jet printing with a pressurised flow. After the removal of unbounded material, the component is sintered in a furnace. By using this method, a density of 99.9% was achieved for Al_2O_3 and silicon nitride (Si_3N_4), [9] and Al_2O_3 and SiO_2 [10]. The disadvantage of the process is the high rate of shrinkage during sintering treatment. Since the amount of shrinkage may vary in different directions, there is concern regarding the geometric accuracy of the final parts.

Furthermore, the process is time consuming because of the required drying time for each layer.

3) Ink-jet Printing

Ink-jet printing is another type of printing process that works without a powder bed. In this method the material feeding is done exclusively via a print head. A semi-liquid mixture of fine particles of ceramic and solvent, called slurry, is fed through the nozzles of a print head and selectively deposited in the form of individual droplets [11]. [12], [13] and [14] attempting to print ZrO_2 through ink jet printing. A flat body with a thickness of 2 mm could be built in these studies. Since this process doesn't have a supportive powder bed, it is only suitable for relief-like structures without overhangs. In addition, the build-up rate of this method is 20.16 mm^3/h [13] which is very slow compared to other AM processes for metallic materials such as the SLM method.

4) FDM

FDM is another AM process used to produce functional thermoplastic models directly from CAD data. The system utilises a controlled extruder-head which squeezes a fine filament of melted thermoplastic through a nozzle. The nozzle deposits the heated plastic layer-by-layer to form the desired shape. The liquid material hardens immediately on contact with the cooler environment. Ceramic-filled thermoplastic filaments are used in the production of ceramic components [15]. The FDM part is a green body that contains 40–45% plastic materials. Subsequently, the part is heated up in a furnace to burn the binder and sinter the ceramic body. As an example, mullite and SiO_2 were produced with this method.

The components showed 8–12% shrinkage during the sintering process. The geometric resolution of this method is limited by the diameter of the extruder nozzle, which in this research was 1.78 mm [15]. A reduction in nozzle diameter to increase resolution results in a lower build-up rate and consequently longer production time.

5) LOM

During the LOM process, thin layers (films) of plastic or paper are fused or laminated together using heat and pressure, and then cut into the desired shape with a computer-controlled laser or blade. For ceramic material manufacturing the film is fed as a rolling process. The ceramic film contains ceramic particles and a significant proportion of binder (e.g. 7 wt% [16]). A post-treatment furnace is needed to sinter final parts and make their body homogeneous. Materials such as silicon carbide (SiC) [17] and Al_2O_3 [16] were tested with this method. The achieved flexural strength for Al_2O_3 parts after sintering treatment was between 145 MPa and 228 MPa. The disadvantages of this method are its relatively low spatial resolution due to excessive film thickness, anisotropic shrinkage during sintering treatment, and delamination of layers. According to the process described in [16] the anisotropic shrinkage has a linear shrinkage of 34% in the X- and Y-directions and 8% in the Z-direction.

2.1.2.1 Additive laser based methods for ceramics

This section gives an overview of the different laser-based AM processes which are possible for the production of ceramic components. Each approach is briefly explained in the following section.

1) Stereo lithography

In this method a 3D object is produced based on selectively curing a photosensitive resin in which a computer-controlled moving laser beam is used to build up structure layer by layer. Ceramic particles are added to thermosetting resin in order to produce a green body of ceramic parts. Afterwards, furnace processes are applied to burn the resin and then sinter the ceramic particles. The proportion of ceramic in the starting materials must be as high as possible to achieve a high density in the ceramic part after sintering treatment[18]. [19] and [18] described their results in producing Al_2O_3 via this method. A high density of 97% and strength up to 275 MPa were achieved in their research [19]. Another group introduced microstereolithography, which uses a layer thickness of 10 microns and correspondingly reaches high geometric resolutions [18]. The main disadvantage of this process is the shrinkage of the materials during sintering treatment, which may limit the geometric accuracy of the final parts. The indicated linear shrinkage is approximately 20%.

2) Selective laser sintering (SLS)

Selective laser sintering (SLS) is an AM process that is used to build solid 3D components. It is a rapid prototyping technique that uses high-power lasers to sinter powder material into solid products layer by layer. There are varied methods

that are summarised under the SLS name. These methods are commonly described as a solid or liquid phase sintering method. The powder bed can be pure ceramic (solid-state sintering) or contain organic or inorganic binders. Some selected SLS processes are as follows:

SLS with binder: In this method ceramic powder layers are selectively solidified with a binder phase. During laser radiation only the binder is melted and the ceramic particles do not melt. One of the variations of this method uses plastic as the binder. The ceramic powder particles are either coated with plastic or the plastic powder is mixed into the ceramic powder. After construction of the body's volume through SLS, the binder is burned in a furnace process which is followed by sintering treatment to achieve a cohesive body of ceramic particles and to increase the density of the solid [20]. I In some cases the plastic binder can also remain in the final parts, such as in bone replacement implants made of hydroxyapatite ($Ca_{10}(PO_4)_6(OH)_2$) where polyamide is used as the binder [21]. Lee *et al.* used oxoborinic acid (HBO_2) as an inorganic binder in the SLS process on a mixture of Al_2O_3 and zinc borosilicate glass ($ZnO\text{-}B_2O_3\text{-}SiO_2$). A bending strength of 19 MPa was achieved for a ceramic–glass composite material after oven curing [22]. Another attempt was carried out to produce a tricalcium phosphate (TCP) ceramic with a glass binder. Here, the temperature was set in the process zone so that the TCP did not melt and decompose, but the glass powder melted and connected to the TCP particles. Production of a solid part was successful, but the mechanical strength of the final part was low [23].

Powder-based solid-phase sintering SLS: In this method the powder materials are sintered together without using any binder. During the process no melting or phase change takes place, and the powder material is merely sintered. Phenix Systems offers an SLS system which is capable of producing Al_2O_3 ceramic components via selective solid-phase sintering. In this case a density of 60% to 65% was reached for final parts after oven curing. The flexural strength of the manufactured components was 15 MPa [24]. Bertrand *et al.* tested ZrO_2 ceramic with the Phenix SLS system. The maximum achieved density was 56%, which is low compared to the theoretical density (Figure 3) [25].

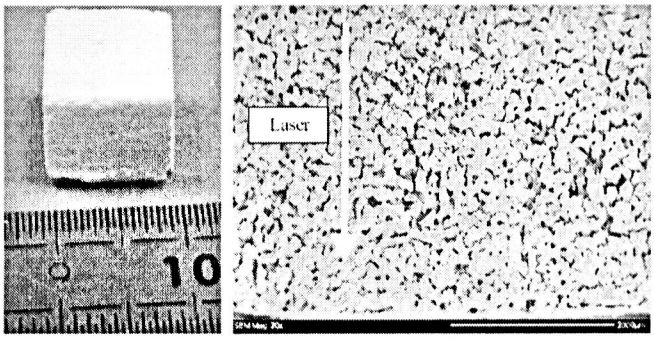

Figure 3 (a) Zirconia cube with 56% density; (b) top view of open porosity [25]

Suspension-based solid-phase sintering SLS: Due to the low density of the powder bed during the solid-phase sintering process, the theoretical density could not be achieved for final ceramic parts. To improve the density of the final components, a laser sintering technology was developed based on ceramic suspension [26],[27]. In this method, instead of using ceramic powder as the feed material, a slip is applied in thin layers and dried. The slip was a water-based solution containing ceramic

powder coated with a polymer as the structure material. The density of the ceramic suspension film is significantly higher than the loose powder layer, resulting in higher-density final parts and consequently greater mechanical properties. For ZrO_2 ceramic material, a density of 78% was achieved.

Melting of a ceramic with glass content using SLS: In the Laser Institute of Central Saxony, so-called "laser micro sintering" was developed to produce parts from an Al_2O_3-SiO_2 mixture [28, 29]. The starting material is a very fine powder with a powder particle size of <1 micron. The powder material is partially or completely melted by a pulse-operated (Q-switched) laser source with a 532-nm wavelength. The produced components had a high geometric resolution and good surface quality. The achieved density is more than 95%, but there are still pores and microcracks in the final parts (Figure 4). By applying a heat treatment, the microcracks can be annealed so that a flexural strength of 120 MPa is achieved [28]. The final parts contain a glass phase of SiO_2 (20 mol%), which means that the components are not pure ceramic materials. This glass phase results in poor mechanical strength that is not suitable for ceramic restoration, such as crowns and bridges.

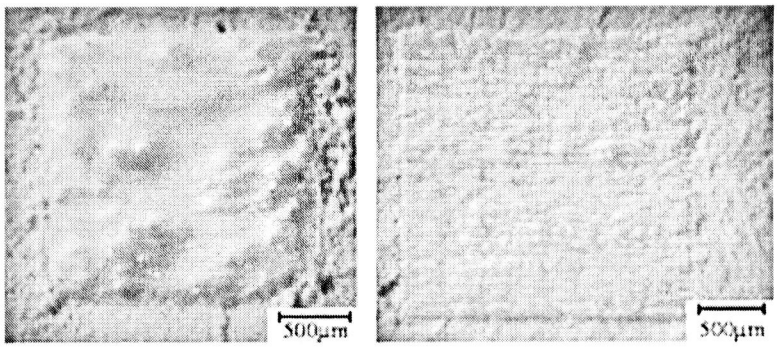

Figure 4 laser sintered patch of ceramic powder[29]

2.2 Selective laser melting (SLM): material research and application

As SLM technology is commercialised in the new millennium, an increasing amount of research work is being carried out as research institutes and universities are able to purchase their own SLM machines. Since the SLM process was designed to produce high-density metallic components, most of the research work done with SLM has been on metals. However, composite materials and ceramics are increasingly gaining interest as they raise the possibility of customising parts' properties according to specific needs and, therefore, expanding the application of this AM technology. Moreover, the development of high-power lasers has also made laser melting of ceramic materials possible.

2.2.1 Metals

Research with SLM on metallic materials has progressed from steel [30] and titanium [31] in its early years to include aluminium [32, 33], copper [34], Inconel [35], magnesium [36], tungsten [37], cobalt-chromium alloy [38] and gold [39].

Most recent research on metals aims to improve the reliability and repeatability of the SLM process via parameter investigations. Building parameters may range from laser power, scanning speed, scan spacing, and even placement of the laser melting layout in relation to the gas flow direction. For instance, Yadroitsev *et al.* carried out a parametric study on the laser power, scanning speed, and scanning direction of the SLM process for 904L steel [40]. Yasa *et al.* experimented with a novel sectorial scanning strategy that reduced the thermal stress of the resultant SLM component. [41]. SLM Solutions GmbH has incorporated this scanning strategy into their machines and named it the "chessboard" strategy. Dadbakhsh *et al.* investigated the effect of the laser melting layout on the SLM of 316L steel cylindrical rods [42]. The effects were related to the temperature gradient induced by the internal gas flow in the building chamber.

Some of the reasons for the keen interest in the SLM technology include its ability to produce high-density parts, its flexibility in manufacturing complex parts otherwise not possible with conventional methods [43] and the possibility of customising production without incurring high tooling costs. Therefore, there is also a large amount of research that focuses on the industrial applications of metallic SLM components in the aerospace [44, 45], automotive [46] and medicine industries [31].

2.2.2 Composites

Research on the SLM of composite materials started with carbide-reinforced copper [47], and polyamide [48, 49]. . In most cases, SLM processing of composite

materials involves melting a mixture of two or more types of powders, with one of the powders acting as the matrix material and the other as the reinforcing particle, usually a ceramic. For instance, titanium carbide has been used with titanium [50], as well as stainless steel [51] to create SLM composite materials. Some innovative methods have involved the in situ formation of reinforcement particles during the SLM process [52].

There are many applications of SLM composite materials, depending on the properties of the composite and the demands of the application. Some research has been motivated by specific applications, such as heat-resistant coatings in engines [53], load-bearing bone implants [54], biodegradable implants [55] and lightweight, high-temperature structural materials [52]. For instance, Shishkovskii *et al.* experimented with hydroxyapatite and nitinol, an alloy of nickel and titanium [56]. This material has the potential to function as a porous implant or drug delivery system, as nitinol has a high strength, high corrosion resistance, good biocompatibility and a unique shape-memory effect. Mumtaz and Hopkinson studied functionally graded ZrO_2-reinforced Waspaloy™, a nickel-based superalloy for high temperature applications, thermal structures, or heat resistant coatings in engines [53]. Dadbakhsh and Hao focused on aluminium-based metal matrix composites for aerospace and automotive applications to exploit the lightweight, high specific strength, and thermal conductivity of aluminium [57].

2.2.3 Ceramics

SLM of ceramic materials has also garnered increasing attention in recent years. Conventional manufacturing techniques of ceramics come with many limitations, such as high tool wear, geometrical inaccuracy due to shrinkage, and high customisation cost. Hence, AM methods capable of producing fully dense parts are of research interest in the processing of ceramics. In a review of the solid freeform fabrication of ceramics in 2003 by Tay *et al.* [58], it was shown that some SLS processes can involve the direct fusion of melted material without the use of any sacrificial binders. In essence, this is similar to the SLM process. However, published papers on the direct sintering or melting of pure ceramics are scarce. The materials have been limited to ZrO_2 and SiO_2.

Employing SLM of ZrO_2 and tri-calcium phosphate (TCP) ceramics for biomedical applications was first introduced by Fraunhofer ILT [59]. Subsequently, yttria-stabilized zirconia (YSZ) [60] and a ZrO_2-Al_2O_3 mixture [24] were also experimented on to test the feasibility of the SLM process for these materials.

One of the major issues for the SLM processing of ceramics is the formation of cracks and delamination due to the high thermal fluctuation that occurs during the process. Hagedorn *et al.* developed a system to solve this problem [61]. A secondary optical system using a CO_2 laser was deployed to preheat the powder bed to 1600°C, and the powders were then melted with a Nd:YAG fibre laser. Dental fixtures with flexural strengths of 500 MPa were attained with this technique [62]. However, the surface finish of the fabricated dental restoration was

poor due to the large melt pool size facilitated by the high preheating temperature, as shown in Figure 5.

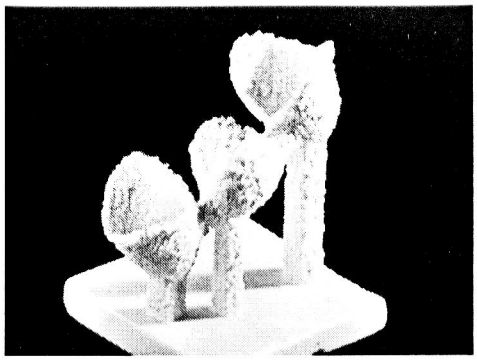

Figure 5 surface finish of dental restoration built by SLM [62]

For research on direct laser sintering/melting of SiO_2, Tang *et al.* achieved the partial melting of SiO_2 powder with a CO_2 laser system [63] and obtained compressive strengths less than 16 MPa. This low compressive strength was caused by the compromised internal structure, which had evident high porosity.

For biomedical applications, SiO_2 is often mixed with other ceramics or minerals, such as hydroxyapatite, feldspar, kaolin, and Al_2O_3. Research work on SLM and direct laser sintering has created SiO_2-based parts for biomedical and dental applications. Liu produced silicate-hydroxyapatite bone scaffolds using a mixture of a hydroxyapatite and SiO_2 slurry [64]. Tian *et al.* studied the effects of a scanning pattern on the stress and mechanical strength of SLM dental porcelain parts. In this study, laser jump patterns, different length-to-width ratios, and laser scan angles were studied with a finite element model. The results showed that

different laser jump patterns have a significant effect on the laser sintering temperature. However, no big difference was seen in the residual stress for different laser scan patterns. The length-to-width ratio of has large effect on the sintering temperature when the same laser parameters and laser scanned area are used. Short scan lines caused high sintering temperatures. The maximum residual stresses were achieved with a ratio equal to 1. Samples with long laser scan lines and a scan angle of 0° showed higher bending strength compared with samples with a scan angle of 90° [65].

Aside from moulding, bone implants, and dental fixtures, the SLM of ceramics also has potential applications in the energy sector. Ceramic materials such as ZrO_2 and ceria (CeO_2) have played a crucial role in the development of fuel cell technology [66, 67]. . SiO_2, with its high melting temperature, low thermal conductivity, and low thermal expansion coefficient, makes an excellent thermal insulator [68, 69]. Combined with SLM's ability to create near full-density freeform solid parts, the SLM of ceramics will bring about a greater variety of applications for ceramic materials.

2.2.4 Powder properties for SLM

Feed materials in SLM technology are in powder form. The size of the powder particles should be in a range of 10 to 60 μm. The existence of huge numbers of powder particles with a size of <10 μm means that the powder flows poorly. Thus, homogeneous deposition of a thin layer is no longer possible. The maximum particle size of a powder depends on the set layer thickness of a SLM process.

Powders with a large particle size have good flowability, which allows homogeneous layer deposition. However, powders with relatively large particles need more input energy to melt. On the other hand, using powders with large particles leads to poorer surface quality and geometric resolution. Furthermore, the particle size of a powder directly contributes to surface roughness. Higher input energy increases the heat-affected zones during the SLM process, which can affect the dimensional accuracy of the parts as well as their surface roughness.

It was suggested that both the surface roughness and dimensional accuracy of final parts can be improved by reducing powder particle size [70]. Spray drying is an efficient and effective powder processing method that is widely used to provide free-flowing powders from micro- and submicrometre-sized powders such as oxides, nitrides, carbides, and borides. The process improves powder flowability by tightening the particle size distribution and creating a spherical agglomerate shape. This method has the advantages of both small particle size and good flowability.

Spray drying a suspension of fine powder particles involves three main steps: first, a peristaltic pump atomises the slurry and feeds a fine droplet spray into a stream of heated gas; second, the liquid is evaporated and the dried solids are left as granules; third, the solid grains are finally collected from the gas stream. The final spray-dried particles are approximately spherical granules with a size range above that of the primary particle size. Another advantage of this method is that it is suitable for the production of a homogeneous powder mixture of various ceramic powders. As homogenous slurry of mixture powder is prepared.

Examples of powder flowability characterisation methods are angle of repose, bulk density, tapped density, Carr's compressibility index, and Hausner ratios. These methods are mainly targeted at specific processes such as storage, compaction, mixing, and volume filling. Thus, it is desirable to measure flowability at flow conditions that are representative of SLM processing situations.

2.3 Dental material:

Dental ceramics are materials that are part of a system which has been designed with the purpose of producing dental prostheses, which are in turn used to replace missing or damaged dental structures. Ceramic materials are a sub group of non-metallic inorganic materials. Ceramics and glasses are brittle, and although they display high compressive strength, they have low tensile strength and may be fractured under very low strain (0.1%, 0.2%). As restorative materials, dental ceramics have disadvantages mostly due to their inability to withstand functional forces that are present in oral cavity. Hence, initially, they found limited applications in premolar and molar areas, although further developments in these materials have enabled their use as posterior long-span fixed partial prosthetic restorations and structures over dental implants [71]. All dental ceramics display low fracture toughness when compared with other dental materials, such as metals [72]. Metal ceramic systems combine both the exceptional aesthetic properties of ceramics and the extraordinary mechanical properties of metals. Some metals used as restorative materials in dentistry may constitute a problem for some patients. These problems may reveal themselves as allergies, gum staining, and the release of metallic ions into the tissue. These drawbacks, as well as the search for more aesthetic materials by patients and dentists, have stimulated the research and development of metal-free ceramic systems.

Ceramics can be classified by their restoration type, as shown in Figure 6. The two major groups are named a) all-ceramic restorations, and b) porcelain-fused-to-metal/ceramics metal systems. All-ceramic materials in dentistry are composed of a

wide range of crystalline phases. We can therefore define ceramics by the nature of the composition of their glass-to-crystalline ratio. The amount and particle size distribution of the crystalline phase determine aesthetic appearance and biomechanical properties [73].

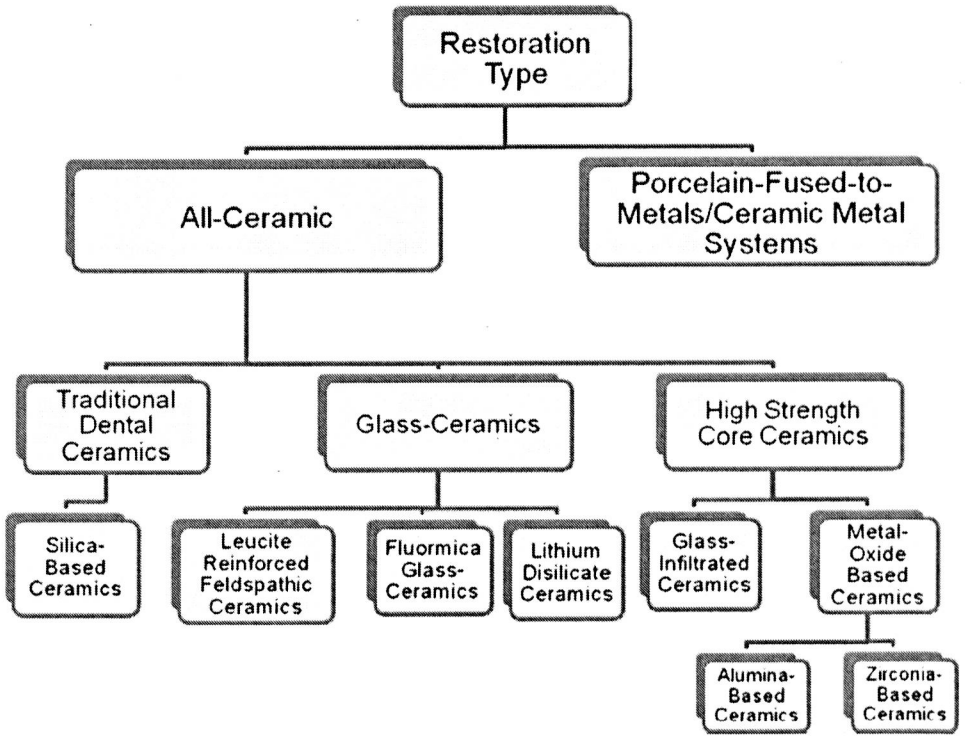

Figure 6 Classification of dental ceramics by the type of restoration [73]

The most traditional type of ceramic is feldspar-based, which contains SiO_2 glasses; "porcelain" is a term often used to describe this type of ceramic because it contains large amounts of SiO_2. So-called "glass ceramics" are different from traditional feldspar-based ceramics because of their larger crystalline phase, which helps stop crack growth and improves mechanical properties. In 1984, the first developed glass ceramic was composed of 55 vol% crystalline tetrasilicic flourmica and 45 vol% glass, and processed through a lost-wax casting technique

[74]. Modern glass ceramics used today include leucite-reinforced and lithium disilicate (LS_2) ceramics. These ceramics contain 45 vol% tetragonal leucite, which dramatically improves flexural strength compared with feldspar-based ceramics.

The next group is crystalline-based systems with glass fillers. Glass-infiltrated, partially sintered Al_2O_3 was introduced in 1988 and marketed under the name In-Ceram. The system was developed as an alternative to conventional metal ceramics and has met with great clinical success. Solid-sintered, monophase ceramics are materials that are formed by directly sintering crystals together without any intervening matrix from a dense, air-free, glass-free, polycrystalline structure. Polycrystalline ceramics, such as ZrO_2 and Al_2O_3, have the highest potential for strength and toughness, which makes them suitable candidates as high-strength frameworks for crowns and fixed partial dentures.

2.3.1 Zirconia (ZrO_2)

ZrO_2 is an oxide ceramic material that possesses high flexural strength and fracture toughness. ZrO_2 has recently been widely used as a structural ceramic due to these privileged properties. In particular in the dental industry, ZrO_2 has become a widespread material for full-ceramic restorations. Pure ZrO_2 has three different crystal structures depending on the temperature. It has a monoclinic crystal phase from room temperature to about 1170°C. From 1170°C to 2370°C a tetragonal phase is stable, and from 2370°C to its melting temperature of about 2710°C a cubic phase is stable [75]. The phases are converted by heating or cooling of the ceramic through these temperatures. The conversion of the tetragonal phase to the monoclinic phase is accompanied by a volume increase about 3–5%. Because of

this property, pure ZrO_2 cannot be produced through a conventional sintering process. The phase conversion during cooling is accompanied by a volume increase, which results in high stress and crack formation. Therefore, ZrO_2 is always used with additives to stabilise the tetragonal phase at room temperature. The common stabilisers are Y_2O_3, MgO, CaO, and CeO. Y_2O_3 is the most common stabiliser for ZrO_2 as it allows the highest flexural strength to be achieved compared with the other additives. ZrO_2 with a 3 mol% Y_2O_3 content has a metastable tetragonal phase at room temperature. This material is referred to as 3Y-TZP (tetragonal zirconia polycrystals). This grade of ZrO_2 achieves a very high fracture toughness and a flexural strength up to 1200 MPa [76]. . Some mechanical and physical properties of conventionally processed 3Y-TZP are summarised in Table 1.

Table 1 Properties of 3Y-TZP ceramics [76]

Flexural strength	800 to 1200 MPa
Fracture toughness	5-7 MPa m1/2
Hardness	12 GPa
Density	6.09 g/cm3
Young's Modulus	210 GPa
Thermal conductivity	2-3 W/mK
Expansion coefficient	10-11×10-6 K-1 (20-800°C)
Melting temperature	2710 °C
Boiling temperature	4300 °C

The value of the flexural strength is recorded for fully dense parts. The bending strength in 3Y-TZP ceramic components will differ depending on porosity, microstructure, and surface roughness.

2.3.2 Alumina (Al_2O_3)

Al_2O_3 is one of the most important technical ceramic materials. Its relatively low cost and the privileged properties of Al_2O_3 have made it one of the most commonly used ceramic materials. Dense polycrystalline Al_2O_3 has a high chemical resistance and good electric insulation properties. Al_2O_3 is also characterised by high wear resistance, hardness, and mechanical strength [75]. Some mechanical and physical properties of conventionally produced Al_2O_3 are summarised in Table 2.

Table 2 properties of Al_2O_3 ceramics [7, 77]

Flexural strength	400 MPa (in the present of porosity the value is lower)
Fracture toughness	3.4 MPa $m^{1/2}$
Hardness	20 GPa
Density	3.92- 3.94 g/cm^3
Young's Modulus	400 GPa
Thermal conductivity	30 W/mK at room temperature 13 W/mK at 400°C 5.5-5.9 W/mK at 1427°C
Expansion coefficient	8.1×10^{-6} K^{-1} (0-800°C)
Melting temperature	2040°C
Boiling temperature	3500°C

Typical applications of Al_2O_3 are substrates for electrical engineering, electronic insulators, transparent burner tubes for lamps, sealing elements in valves, components for pumps, cutting ceramics, and medical implants.

2.3.3 Alumina toughened Zirconia (ATZ)

A material made of ZrO_2 with a content of Al_2O_3 is often called an alumina-toughened zirconia (ATZ). Most commonly, the mixture contains 80 wt% ZrO_2 and 20 wt% Al_2O_3, in which the ZrO_2 is partially stabilised with Y_2O_3. The mechanical properties of the 3Y-TZP are improved by adding Al_2O_3. Moreover, Al_2O_3 causes a reduction in weight and increases the elastic modulus and flexural strength of 3Y-TZP up to 2400 MPa. The microstructure of the ceramic mixture is biphasic, with a grain size usually of <1 micron metre. ATZ is a relatively new product that was developed few years ago. Some mechanical properties and physical properties of ATZ are summarised in Table 3.

Table 3 properties of ATZ [78]

Flexural strength	1200 to 2400 MPa
Fracture toughness	8 MPa $m^{1/2}$
Hardness	14-15 GPa
Density	5.5 g/cm^3
Young's Modulus	220 GPa
Thermal conductivity	6 W/mK
Expansion coefficient	9×10^{-6} K^{-1} (20-800°C)
Melting temperature	1860 °C

Some potential applications of ATZ ceramics are highly stressed wearing parts, orthopaedic implants such as joint implants, ceramic membranes in fuel cells, and many of the ZrO_2 ceramic applications that have already been mentioned.

Chapter 3: Methodology

3.1 Experimental approach

Laser melting of Al_2O_3-ZrO_2 mixtures is a new area in the material research of SLM. Hence, the approach of the experiment is a series of progressive tests, from one-dimensional (1D) single-track melting, to two-dimensional (2D) single-layer melting, and finally to the automated fabrication of 3D blocks.

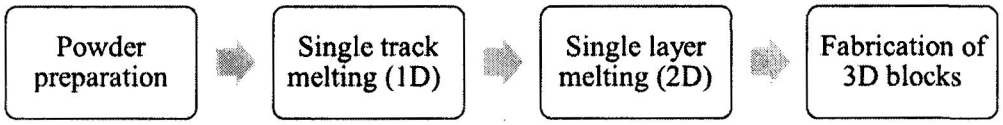

Figure 7 Flowchart of approach of experiment

The goal of the 1D single-track melting test was to determine if the laser melting of ceramic powder with an ytterbium fibre laser (λ = 1.07 μm) is feasible and to study the combination of laser power and scanning speed suitable for the process. The results would be used as a reference for subsequent tests.

In the 2D single-layer melting, an additional factor was to be included: hatch spacing. Hatch spacing is defined as the distance between the centrelines of two adjacent laser scanning lines, as illustrated in Figure 8.

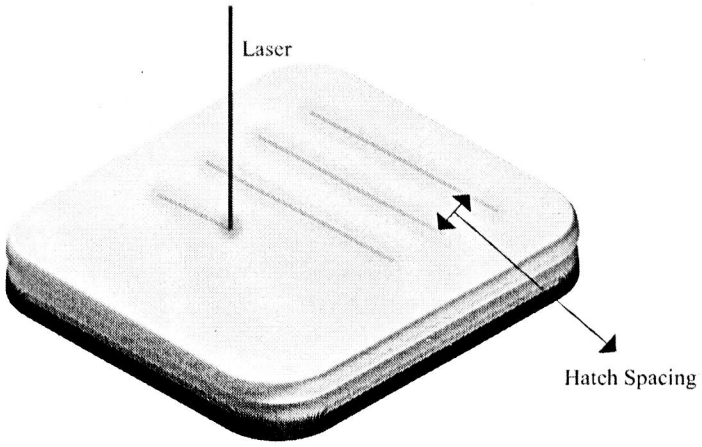

Figure 8 Sschematic of hatch spacing concept

The process parameters for fabricating 3D ceramic blocks would come from the results of the 1D and 2D laser melting of the ceramic. In 3D fabrication, the additional parameter is the layer thickness.

Two ZrO2-Al2O3 powders were selected as the ceramic powders for this study. Flowability of the powdered material is crucial in SLM, and can be improved by spray drying. Therefore, the spray-drying method was applied on the powder mixture to prepare a highly flowable powder suitable for the SLM process. The flowability of the spray-dried powder was investigated and benchmarked against the original powder and industrial spray-dried powder. In this flowability investigation, a powder characterisation method is used that provides information regarding the dynamic behaviour of the powder flow.

Material characterisations tests were carried out for the powder material and laser melted specimens through XRD, field emission scanning electron microscopy (FESEM), and SEM/energy-dispersive X-ray spectroscopy (EDX). XRD tests and FESEM image capturing were carried out using a PANalytical Empyrean and

JOEL JSM 7600F, respectively, in Material Laboratory 1 of the School of Mechanical and Aerospace Engineering (MAE) at NTU.

3.2 Powder preparation

3.2.1 Materials

Commercially available Al_2O_3 with a purity of 99.8% and particle size distribution <5 μm with an average particle size of 3 μm, supplied by Industrial Powder Company, USA, and 3 mol% Y_2O_3-stabilised ZrO_2 nano powder (30–60 nm) with a purity of 99.95+% procured from Inframat Advanced Material, LLC was used. The powders were mixed together in the eutectic ratio. According to the Al_2O_3-ZrO_2 phase diagram, the eutectic composition is at Al_2O_3 to 37 mol% ZrO_2 (58.5 wt% Al_2O_3 to 41.5 wt% ZrO_2). As Figure 9 illustrates, a substantially lower melting temperature of 1860°C is required for this material ratio compared with each individual phase [79]. This helps to facilitate melting during the SLM process. This Al_2O_3-ZrO_2 mixture ratio provides several advantages compared with the individual components. The melting point of this mixture compared with Al_2O_3 and ZrO_2 individually is reduced from 2710°C and 2010°C, respectively, to 1860°C. Less energy is required to fully melt the mixture during the SLM fabrication process. At high temperatures, this mixture also exhibits superplasticity behaviour [80] which reduces the stress built up during the rapid melting and solidification process in SLM. The mechanical properties of this Al_2O_3-ZrO_2 mixture are also better than the individual components and, lastly, a fine-grained structure is formed at the eutectic point in SLM-fabricated parts using this mixture.

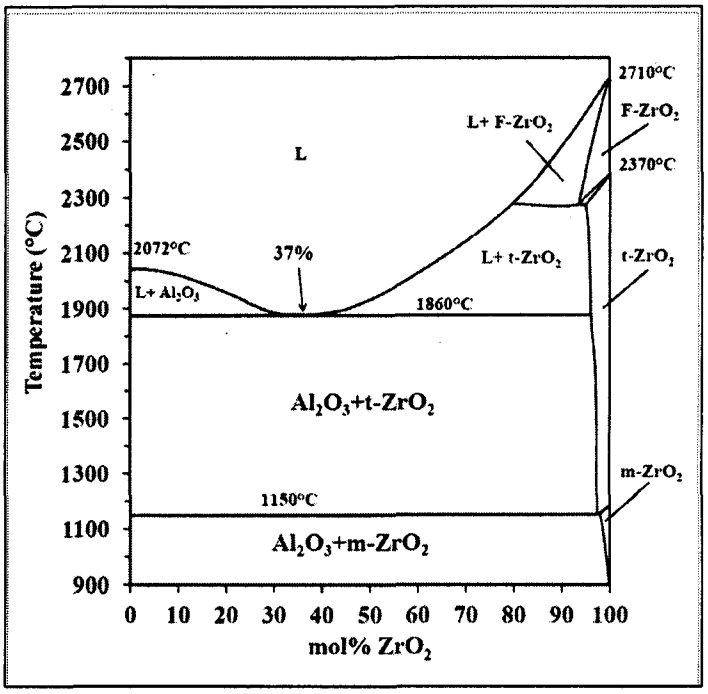

Figure 9 phase diagram of alumina zirconia system

3.2.2 Spray drying method

The eutectic mixture powder was dispersed in an aqueous medium to form a slurry of solid loading 40 wt%. 1 wt% Dolapix CE64 (Zschimmer & Schwarz, Germany) as a dispersant and 1 wt% polyvinyl alcohol (PVA) as a binder were added to the slurry. In order to obtain a homogenous slurry, the suspension was milled for 20 h in a ceramic jar with 10 mm and 25 mm grinding balls. Using a standard spray dryer (Labplant, UK), the prepared aqueous slurry was spray dried. The spray-drying process involved three main steps: first, a peristaltic pump delivered the slurry through a small diameter jet, which caused the liquid to emerge as fine atomised droplets, and sprayed it into a stream of heated gas; second, the liquid is evaporated and the dried solids are left as granules; third, the solid grains

are finally collected from the gas stream. A schematic of the spray-drying process is shown in Figure 10 . To optimise the spray-drying process, a hot air inlet temperature of 140°C and pump speed of 5 ml/min were set in the spray dryer machine. A nozzle diameter of 0.5 mm was used in the system.

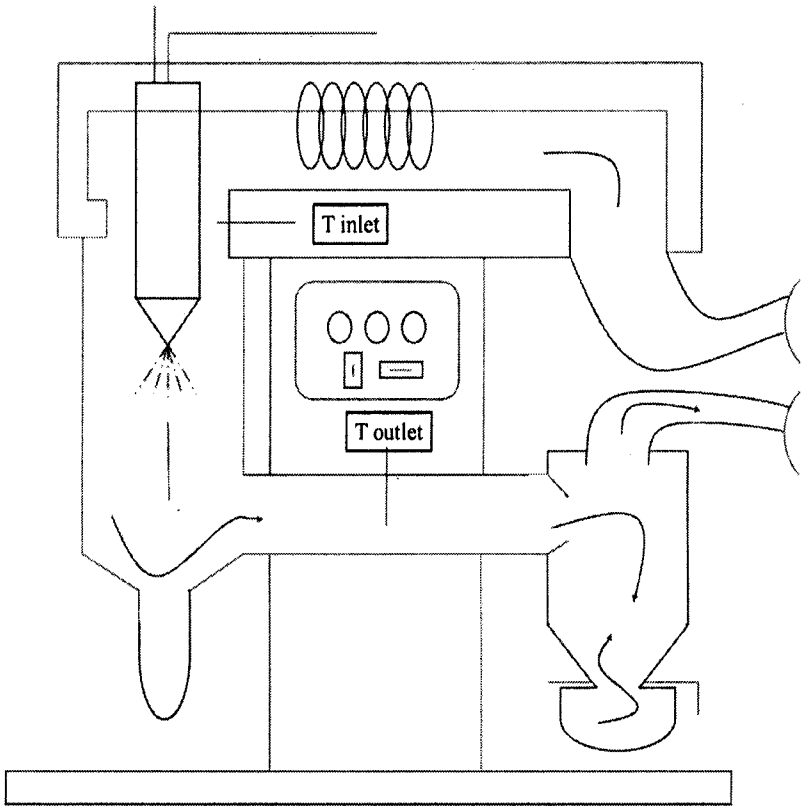

Figure 10 Spray drying schematic

A heat treatment process at 600°C for 2 h was conducted after the spray drying. The PVA present in the spray-dried powder decomposed and ran from the powder during the heat treatment process, providing a pure ceramic powder.

3.2.3 Flowability test

The Revolution Powder Analyser manufactured by Mercury Scientific Inc. was used in the experiments. The device consists of a rotating drum with an image

acquisition system, as illustrated in Figure 11. The drum is made of aluminium with an inner diameter of 55 mm and a width of 35 mm. One side of the drum has a transparent window to allow the image acquisition system to monitor the powder behaviour inside. The drum speed can differ from 0 to 200 rpm. The backlight source helps to determine the powder surface boundary and cross-sectional area of the powder. The flowability test is achieved by monitoring the discrete behaviour of powder based on the sequence of avalanches at low rotating speeds.

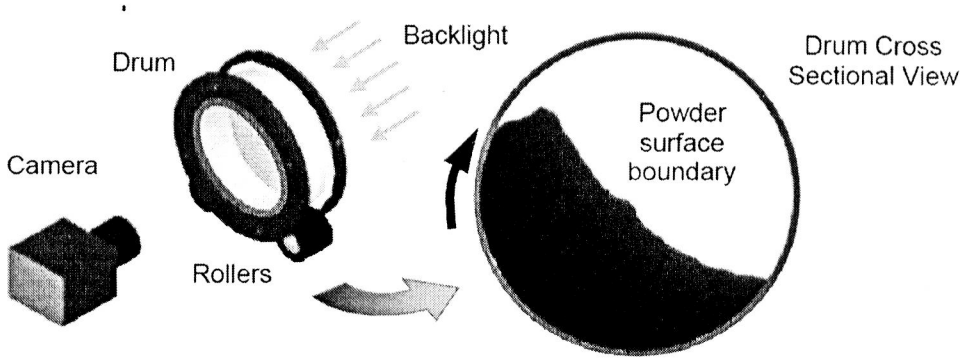

Figure 11 schematic of rotating drum and image acquisition system

This dynamic method is based on the avalanche angle test. The powder should move up the drum wall as the drum rotates until the friction between the powder and drum wall is overcome by the weight of the powder, causing the powder to slide and flow off the drum wall, resulting in an avalanche phenomenon [81].

The following characterisation indexes are developed according to the recorded data by the acquisition system:

Avalanche angle: the dynamic angle of repose or angle of avalanche is the angle between the flowing powder and the horizontal base just before the avalanche

occurs (Figure 12).). The angle obtained from a linear regression of the powder surface boundary at the maximum potential energy just before avalanche phenomenon occurs. As a matter of fact, powders with higher avalanche angles show poorer flowability.

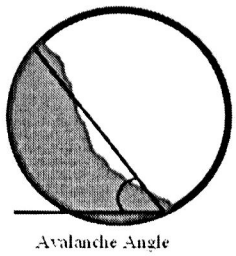

Figure 12 Schematic of the measured avalanche angle

Surface fractal: the fractal dimension of powder-free surface determines the roughness of the powder surface or surface linearity, which is an indication of surface smoothness. This index is measured after each avalanche occurs to show how the powder particles are rearranged. Powders with a smooth surface have a lower fractal surface value compare to powders which have rough and uneven surfaces (Figure 13). For applications requiring an even powder distribution, such as SLM, the closer the surface fractal is to one the better the powder will perform.

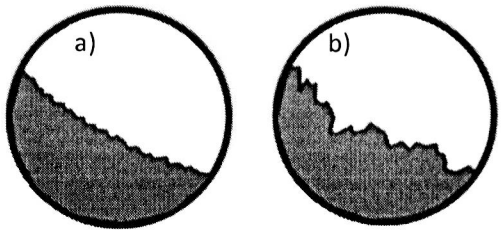

Figure 13 Schematic of surface fractal a) near1 b) bigger than one.

3.3 Experimental procedures

3.3.1 SLM equipment

In Nanyang Technological University (NTU), a customised SLM® 250 HL was available in the Singapore Institute of Manufacturing Technology (SIMTech)-NTU Joint Laboratory on 3D AM. The machine has two separate laser modules. Laser 1 has a Gaussian laser beam (standing beam diameter of 80 μm), with a maximum power of 400 W. Laser 2 has a uniform beam (standing beam diameter of 730 μm) with a maximum power of 1000 W. The ytterbium fibre lasers have a wavelength of 1.07 μm.

The SLM process is fully automated, but requires data preparation by the user. Before the process starts, 3D CAD data is required, commonly in the <.STL> file format. The 3D digital model is oriented in the build-up position and the file is sliced layer by layer to yield the layer scanning information.

The process starts with a powder coating system that transfers a thin layer of powder and evenly distributes it to the building platform. Once the powder is distributed, the laser scans the powder bed according to the slice data and melts the powder selectively. The building platform is then lowered depending on the user's specification, and the next layer of powder is transferred. These steps are repeated until a complete 3D part is built. The unmelted powder can easily be removed and most of it can be reused after sieving. Figure 14 shows a schematic of the SLM process similar to the machine used in this study.

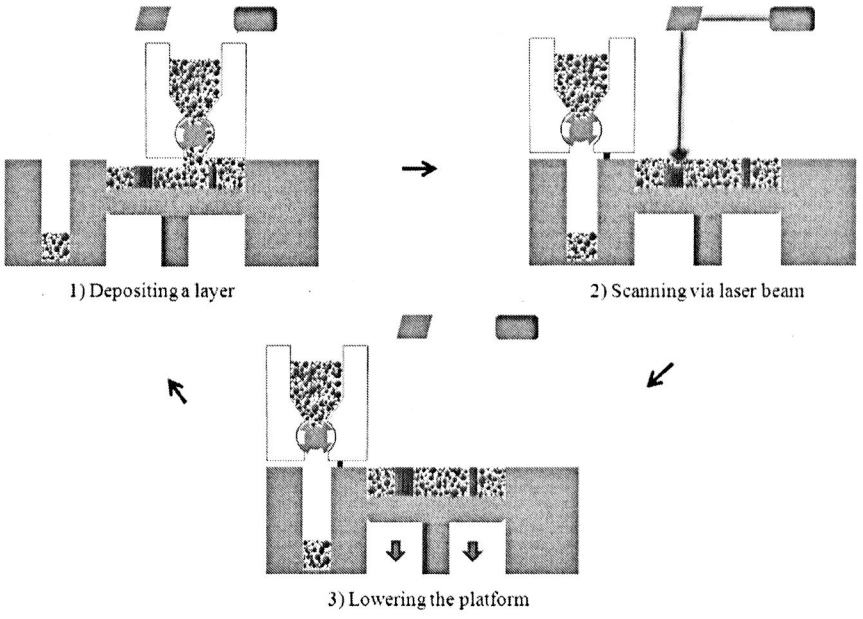

Figure 14 schematic of SLM Process

3.3.2 Material characterisations

Material characterisations were carried out for the powder materials and laser-melted specimens with XRD, FESEM, and EDX analysis. XRD tests and FESEM image capturing were carried out using a PANalytical Empyrean and JOEL JSM 7600F, respectively. XRD analysis and FESEM were conducted to study the phases and morphology change of the powder before and after spray drying. The SLM parts were analysed with XRD, FESEM, and EDX to investigate the parts' morphology and chemical composition changes during laser processing.

Density measurement: The densities of the SLM fabricated Al_2O_3-ZrO_2 3D blocks were determined based on Archimedes' principle by measuring the mass of the sample in the air and the mass of the sample immersed in liquid. In this test, distilled water with a density of approximately 1000 kg/m^3 at room temperature

was used as the immersion medium to measure the sample density. The equipment is shown in Figure 15. The density of the sample is calculated using the value of mass obtained with the equation shown below:

$$D_s = \frac{M_{air} \times D_{water}}{M_{air} - M_{water}} \quad (1)$$

D_s = density of the sample

D_{water} = density of the distilled water

M_{air} = mass of the sample in the air

M_{water} = mass of the sample in the distilled water

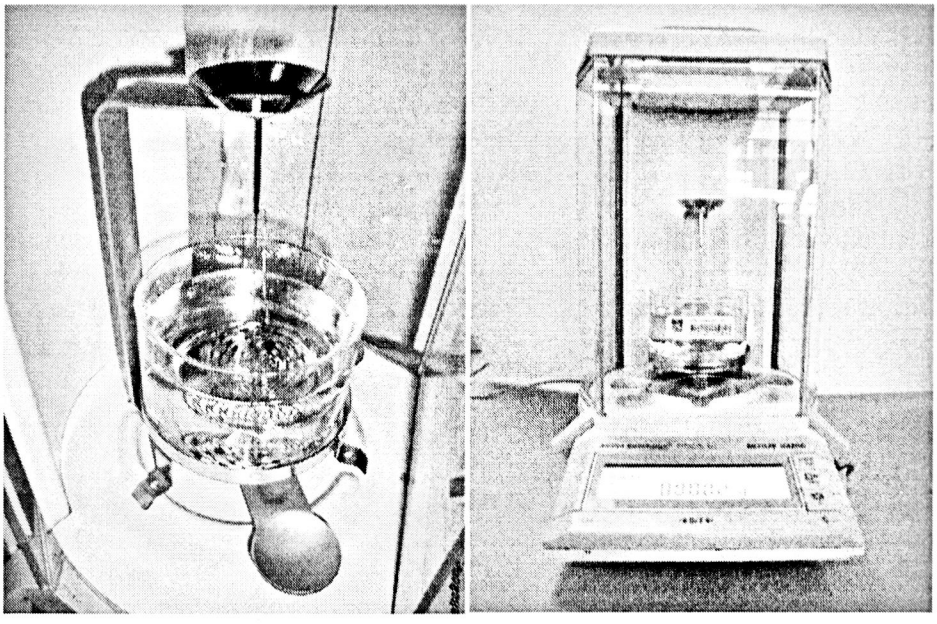

Figure 15 Density measurement equipment setup – Mettler Toledo AG204 Delta Range

3.3.3 Single track melting

The experiments using the Al_2O_3-ZrO_2 mixture powder in the SLM machine were started with single-track melting to demonstrate whether melting of the ceramic

mixture power with the ytterbium fibre laser was possible. The ceramic particles would melt and bind together if the input energy density was sufficiently large. Laser energy density is a factor that indicates the energy input in the SLM process. Laser energy density, E_ρ, is defined by the laser power, P (W), laser scanning speed, u (mm/s), and laser beam diameter, δ (mm) in the equation below:

$$E\rho = \frac{P}{u\delta} \ (J/mm^2) \tag{2}$$

Depending on the laser beam properties, the input energy density needed to melt ceramic powders will vary. This is because of the laser–material interaction changing when the laser is different. The used SLM machine in this study has two fibre lasers with different laser beam distribution patterns, maximum laser power, and laser beam diameters. Laser 1 has a Gaussian distribution with a maximum laser power of 400 W and a laser beam diameter of 80 μm. Laser 2 has an even distribution with a maximum laser power of 1000 W and a laser beam diameter of 730 μm. Juste *et al.* showed in their study that 16 J/mm^2 is needed to melt a ceramic powder with a laser beam diameter of 69 μm [82].

The first phase of the experiments was a single-track melting, which was used as a guideline to determine the best range of process parameters for both Laser 1 and 2. This helped to narrow down the combination of laser power and scanning speed suitable for the next part of the experiments. The combinations of laser power and scanning speed for Laser 1 and 2 are shown in Tables 4 and 5, respectively.

Table 4 Scanning parameters for single track melting of alumina-zirconia powder via laser 1

Laser power (W) / Scanning speed(mm/s)	10	50	100	150	200
100	X11	X12	X13	X14	X15
200	X21	X22	X23	X24	X25
300	X31	X32	X33	X34	X35
400	X41	X42	X43	X44	X45

Table 5 Scanning parameters for single track melting of alumina-zirconia powder via laser 2

Laser power (W) / Scanning speed(mm/s)	5	10	20	50	100
400	Y11	Y12	Y13	Y14	Y15
600	Y21	Y22	Y23	Y24	Y25
800	Y31	Y32	Y33	Y34	Y35
1000	Y41	Y42	Y43	Y44	Y45

3.3.4 Single-layer melting

The second part of the experiments includes building a single 10 mm × 10 mm layer of Al_2O_3-ZrO_2 powder. The results of the chosen process parameters from the previous part of the experiments weren't applicable for scanning a single layer. This is because the level of input energy for single-layer scanning was too high, which meant that the samples were burnt. Therefore, different scanning parameters were set for the experiments. For Laser 1 the tested parameters were in the range of 100 to 1000 mm/s for the scanning speed and 200 to 400 W for the laser power.

For Laser 2 the parameter changed from 100 to 700 mm/s for the scanning speed and 200 to 950 W for the laser power.

Another scanning parameter that was changed during the experiments was hatch spacing, which is the distance between two adjacent scanning lines. The hatch spacing ranged from 0.06 to 0.26 mm for Laser 1 and 0.05 to 0.5 mm for Laser 2.

3.3.5 Fabrication of 3D blocks

In the third experiment, the goal was to build 10 mm × 10 mm × 10 mm 3D Al2O3-ZrO2 blocks. The laser scanning parameters were based on the results from the single-layer melting of Al2O3-ZrO2. In the experiment with Laser 1, the layer thickness used was 100 μm. The results with Laser 1 showed that this laser is not able to produce coherent plates with a thin layer thickness. Hence, the fabrication of 3D parts continued with Laser 2 using a layer thickness of 500μm. The hatch spacing was 400 μm, which means that there was an approximately 50% overlap between two scan lines.

Chapter 4: Results and discussion

4.1 Powder characterization

4.1.1 Powder morphology

Scanning Electron Microscopy (SEM) was used to analyze morphology of initial powders before spray drying and spray dried powder. Moreover, two zirconia and alumina spray dried powders were supplied from industry to compare the flow behaviour of these powders. Figure 16 illustrates the SEM pictures of each powder. Figure 16 (a) and (b) show the initial alumina and zirconia powder in submicron size < 5 μm and Nanosize respectively. So both powders are of small sizes which negatively affect the overall blend flowability. The fine particle size results in high surface energy which maintains a high van der Waals attraction among particles and in turn prevents them from free flowing. The particle shape of these powders is mostly spherical but there are so many irregular shape particles that cause poor flow behaviour in the powders. Figure 16 (C) illustrates the powder mixture after spray drying. Spray drying process was successfully applied to granulate the small particles together and form larger spherical granules. Particularly, spray drying changed the powder particle size from < 5 μm to <50 μm. The larger particles with spherical shape are expected to improve the flowability of powder.

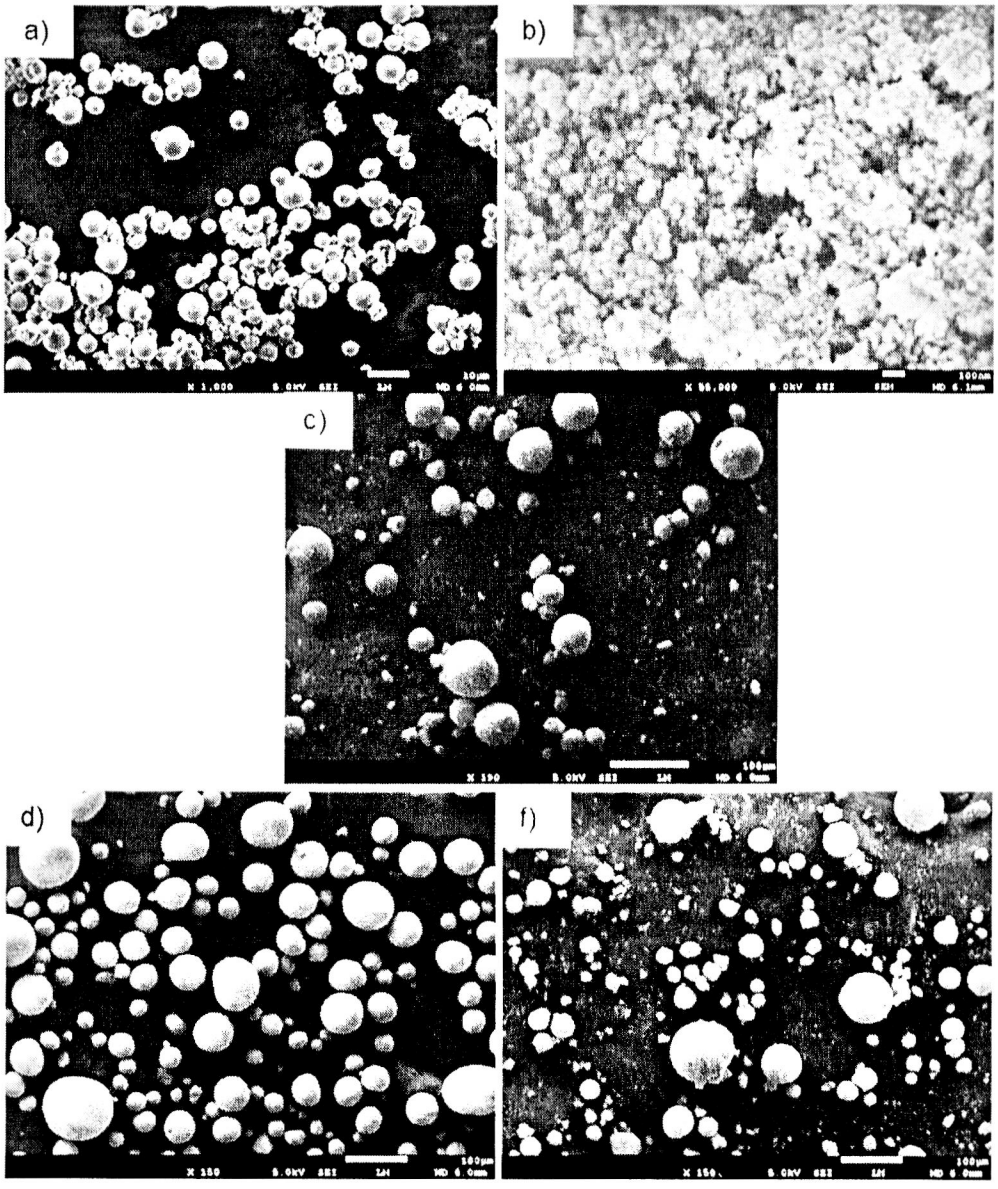

Figure 16 SEM pictures of a) Submicron alumina b) Nanosize zirconia c) Spray dried powder of alumina-zirconia mixture d) Spray dried alumina from industry f)Spray dried zirconia from industry

Figure 16 (d) and (f) show the spray dried alumina and zirconia powder respectively that supplied from industry. Smooth particle surface and bigger particle size of 50-90 μm are expected to show better flow behaviour compared to spray dried powder prepared in lab.

4.1.2 Phase analysis

XRD patterns of powder mixture before and after spray drying are illustrated in Figure 17. Results revealed that alumina and zirconia are the major phases. In addition, no phase change was observed during spray drying process.

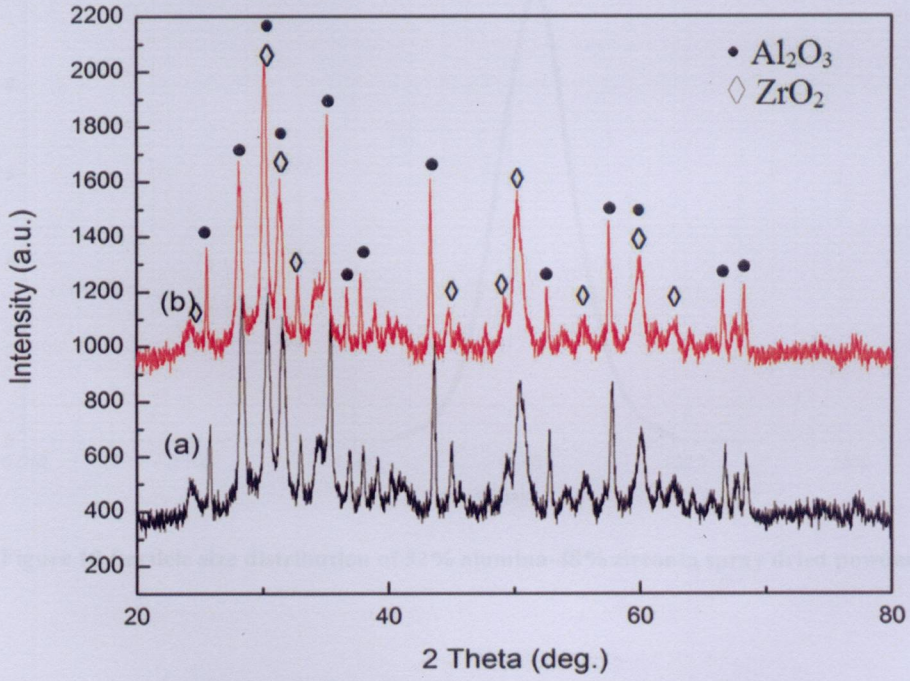

Figure 17 XRD patterns of powder mixture (a) before spray drying (b) after spray drying.

4.1.3 Particle size distribution

Laser Scattering Particle Size Distribution Analyzer LA-950 was used to determine the particle size distribution of spray dried powder. The results were expressed in both Range analysis and cumulative form. In Range analysis each size range is listed in order as shown in Figure 18. Range analysis is suitable to seek a particular size of ideal mid-range size, while cumulative analysis is used to determine the amount of under size or over samples.

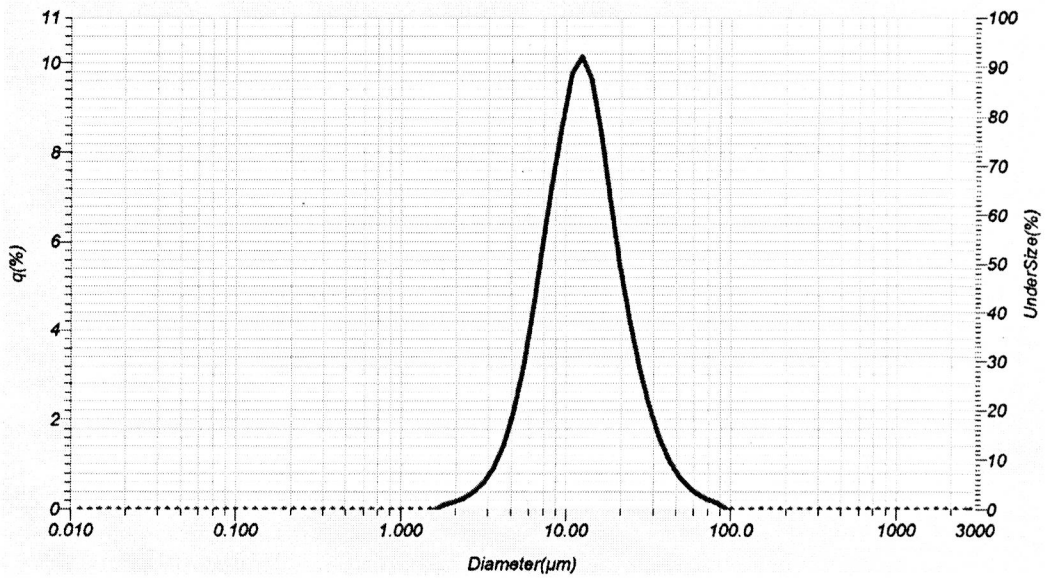

Figure 18 Particle size distribution of 52% alumina-48% zirconia spray dried powder

The mean size of sample is 14.8 microns which is indicated the central point of symmetric distribution. The Median values of samples are as follow Dv0.1: 6.02 μm, Dv0.5:12.33 μm and Dv0.9: 26.14μm. Median values are defined as the

percentage where amount of the population resides below this point for example 90% of particles are below 26.14 μm size.

4.2 Flowability test

Figure 19 shows the cumulative avalanche angle distribution of all powders. The X-axis and Y-axis are Avalanche Angle (degrees) and Fraction of total avalanches respectively. Sample 1 is a mixture of submicron alumina powder and zirconia nano powder prepared in-house. Sample 2 is the spray dried mixture powder of sample 1 and sample 3 is the mixture of alumina zirconia spray dried powders supplied from industry.

Low avalanche angle values coupled with a narrow value distribution are correlated to a powder with better flowability. Thus spray dried powders (sample 2&3) show better flow behaviour compared to powder mixture before spray drying (sample1). This is the result of bigger size of the particles with near spherical shape. Finally sample 3, spray dried powder from industry, shows better flowability compared to sample 2 (in-house spray dried powder) due to smoother surface of particles.

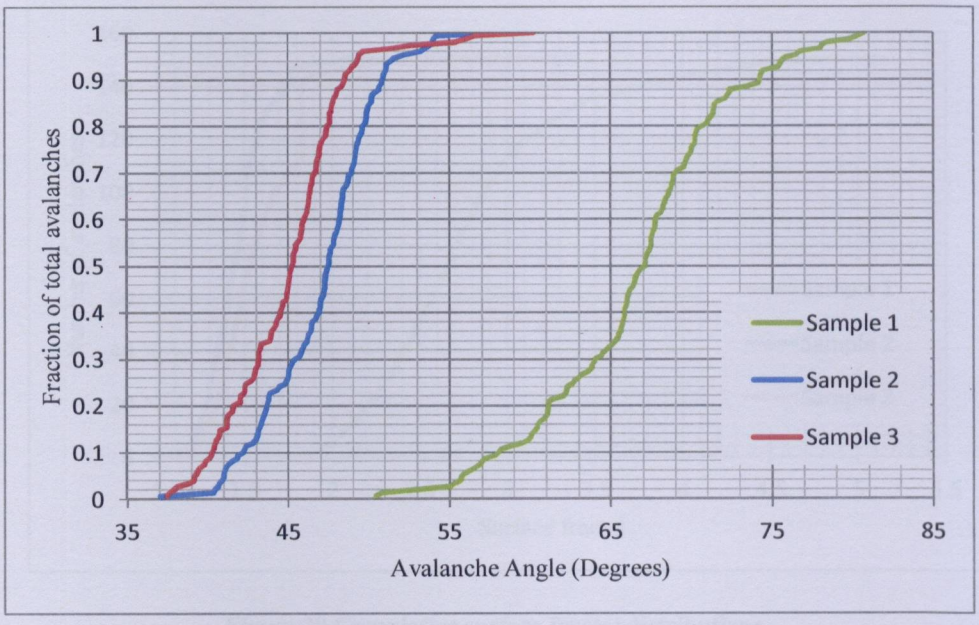

Figure 19 Cumulative avalanche angle distributions

The results of surface fractal versus number of avalanches are shown in Figure 20. The surface fractal is an indication of deviation of the powder surface position from the centre-line. It is calculated based on the mean-square error between the surface position and the average lineas. It is formulated

$$L=1/(1+\sigma) \quad (3)$$

where σ is the standard deviation of the surface from the center-line.

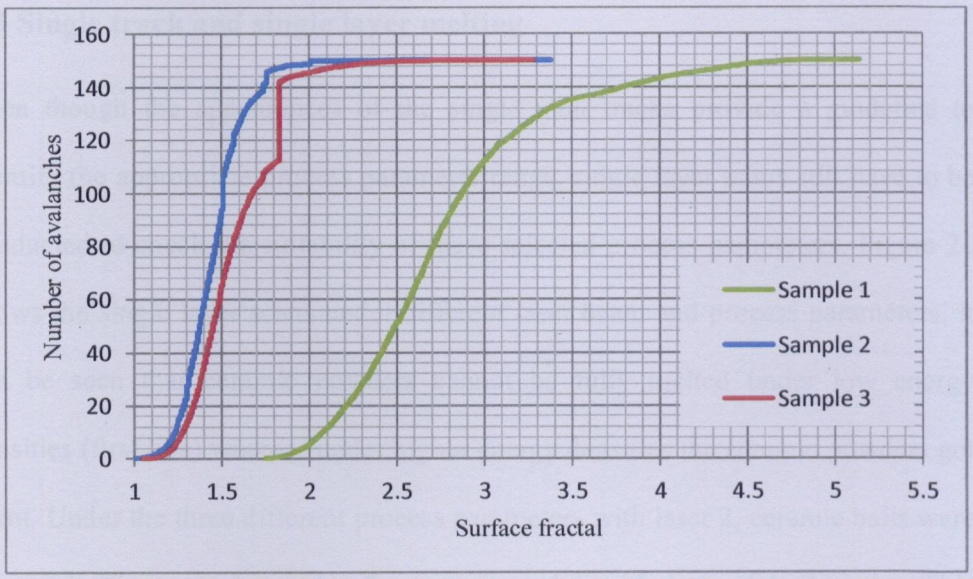

Figure 20 Cumulative surface fractal distributions

The results indicate the generated boundary of powders free surface after avalanche occurrence to present structured or uneven surface that can affect powders packing. Also higher surface linearity of fractal surface near to 1 indicates low tendency of agglomeration in the powder. In the SLM process, low degree of agglomeration in the powder would enable the system to deposit a thin layer of powder evenly on the building platform. Sample2 illustrates lower surface fractal that means this powder can reorganize itself better than the others. This concern is correlated to the SLM powder deposition process. Thus, during SLM process sample2 can be deposited more packed and even. This is due to wide range of particle size distribution that increases the packing density of powder.

4.3 Single track and single layer melting

Even though the appearances of the single melt tracks provide a guideline to identify the appropriate process parameter range, single layer scans still have to be conducted to check the suitability of these selected process parameters. Figure 21 shows the single layer scans under different laser beam and process parameters. It can be seen that ceramic powders cannot be fully melted under low energy densities (first line) whereas under higher energy densities the ceramic powders got burnt. Under the three different process parameters with laser 2, ceramic balls were observed. The melted powder forms separated liquid drop of ball shape. This molten material was fully contained by loose powder instead of fully dense material, that cause the tensile traction on the melt was not sufficient to confine it to a continuous geometry. This phenomenon is called balling. Melt pool commonly refers to the small-sized portion of a work piece where the material has reached its melting point and melted locally due to laser radiation. During this experiment the melting occurred but the melt pool was too big, which caused the melted liquid phase wets the surrounding ceramic powder. In this situation the molten materials contain loose unmelted powder which causes balling effect. One reason for the formation of large melt pools is overheating of materials. If the first line of scanned material is still in liquid state as the second track is being scanned, the molten particles will join and form balls. Another possible reason for balling to occur is due to low wettability of molten ceramic on the stainless steel platform. As the molten ceramic is unable to stick onto the base plate, ceramic balls are formed.

Therefore, to increase the wettability of the molten ceramic with the building platform, the stainless steel platform is replaced with a ceramic plate (alumina).

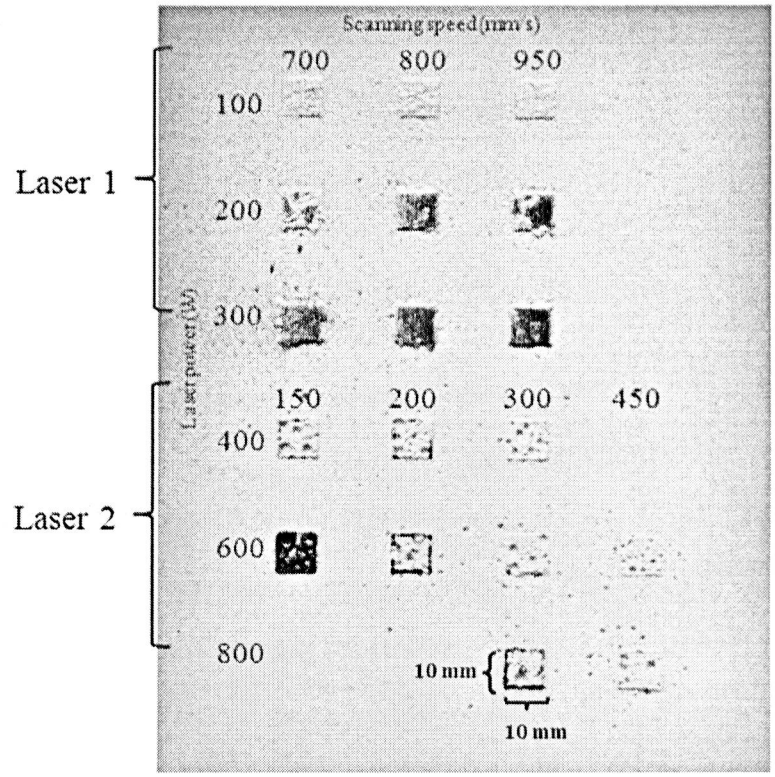

Figure 21 Results and process parameters of scanned ceramic powder (I)

On the other hand, the scanning speed was also increased in an attempt to eliminate the balling phenomenon. According to this test, the best P/ V ratio (laser power P, scanning speed V) for laser 1 was in the range of 0.28 - 03 and for laser 2 was in the range of 1.3 - 3.

Despite increasing the scanning speed, balling still occurred for laser 1 and laser 2. Hence, the hatch spacing is now modified. As most of the samples were burnt for laser 1, hatch spacing was increased to 0.06, 0.1, 0.14 mm. Two different hatch spacing were tested for laser 2, one lower than previous hatch space 0.3 and another higher 0.5 (Figure 22).

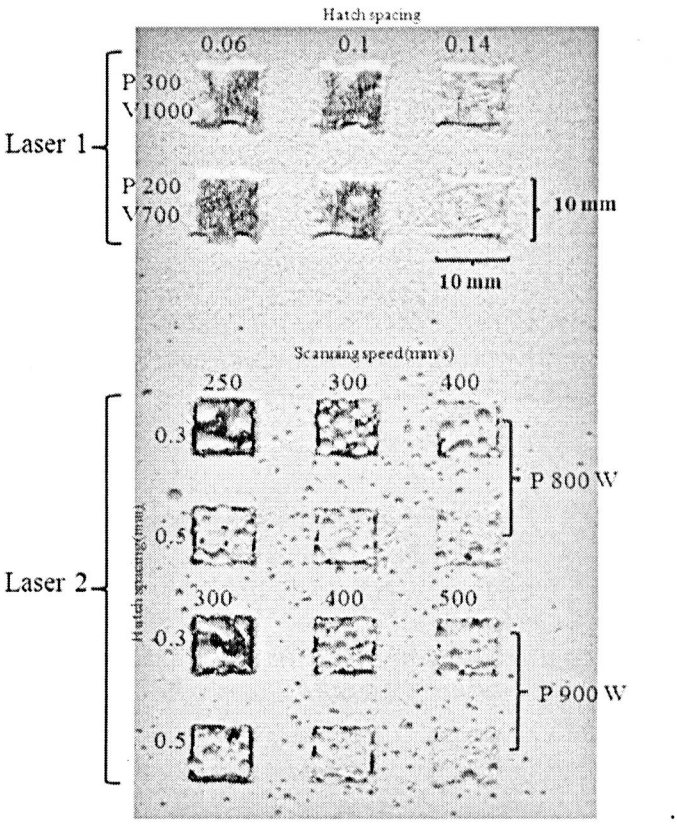

Figure 22 Results and process parameters of scanned ceramic powder (II)

Figure 23 indicates two samples with same laser power (800 W) and scanning speed (250 mm/s) but different hatch spacing (0.3 mm right, 0.5 mm left). As can be seen in the picture, balling phenomenon reduced with lower hatch spacing (0.3 mm) in laser 2, so the experiments continued with decreasing hatch spacing to produce more uniform ceramic layer.

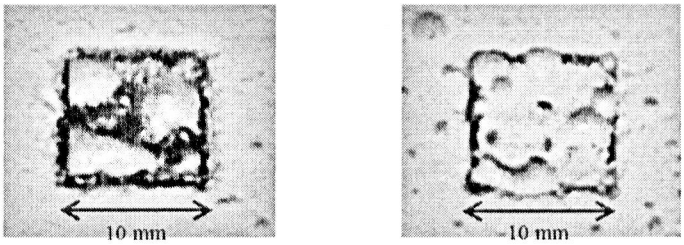

Figure 23 Balling phenomenon in scanned samples with different hatch spacing

This next series of process parameters with new hatch spacing value is shown in Figure 24. With these new parameters, a single layer of ceramic material can be built under 0.1 and 0.2 mm hatch spacing via laser 2, Figure 25. These single layers are of large thicknesses due to high amount of powder laid on the building platform. The lowest layer thickness that can be achieved with used powder was 1 mm.

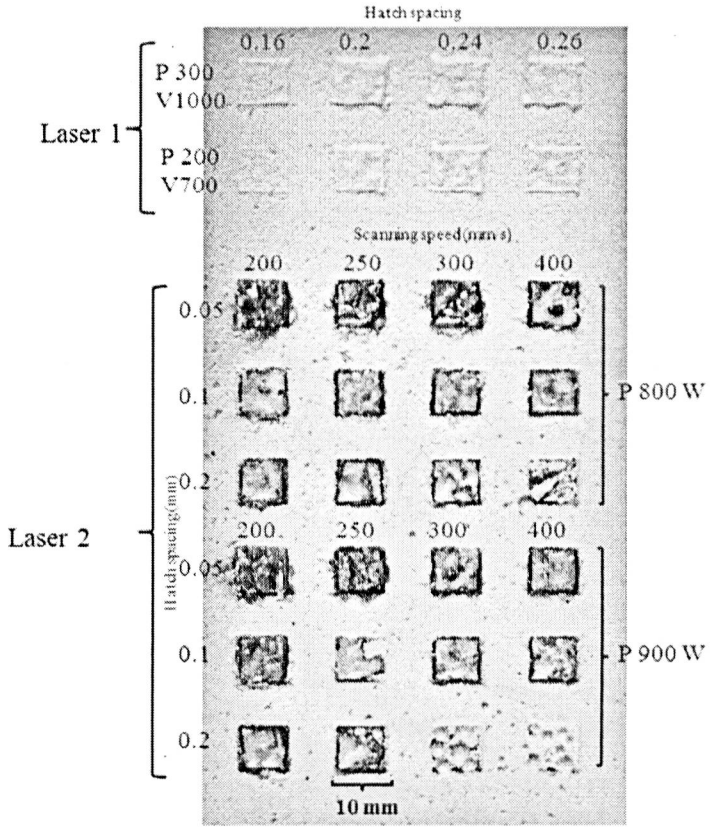

Figure 24 Results and process parameters of scanned ceramic powder (III)

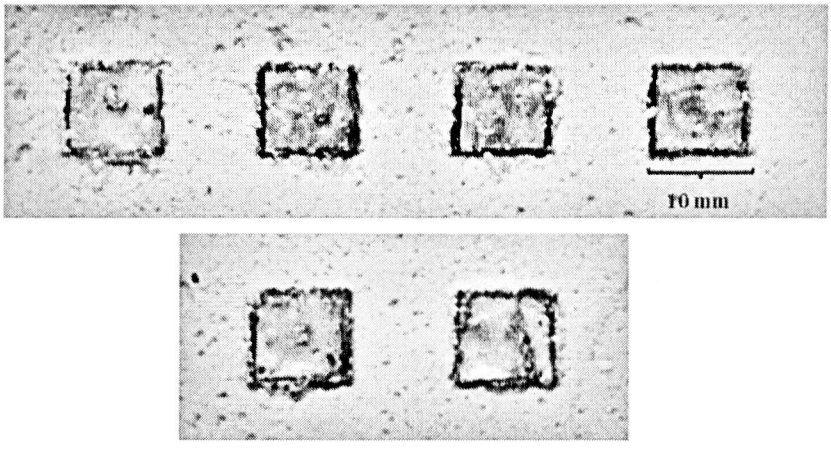

Figure 25 Fabricated ceramic single layer via SLM

Figure 26 shows the SEM pictures of fabricated single layer from alumina-zirconia powder under two different magnifications. Figure 26(a) shows the single layer at a lower magnification. A crack free layer was observed and can be achieved by fully melting the ceramic powders. However, the surface of this ceramic layer is not completely smooth. This is because of overheating of materials during the fabrication process.

Figure 26(b) shows the ceramic single layer under a higher magnification. The pearlite-like structure can be seen in this picture (the red circle in the picture). Pearlite is a two- phased layered structure that occurs in eutectoid composition. It is a very common eutectic microstructure that forms during slow cooling rate. This structure is one of the strongest structural bulk materials. So it can be concluded that eutectic mixture of alumina- zirconia powder is completely melted and slowly cooled to form pearlite structure.

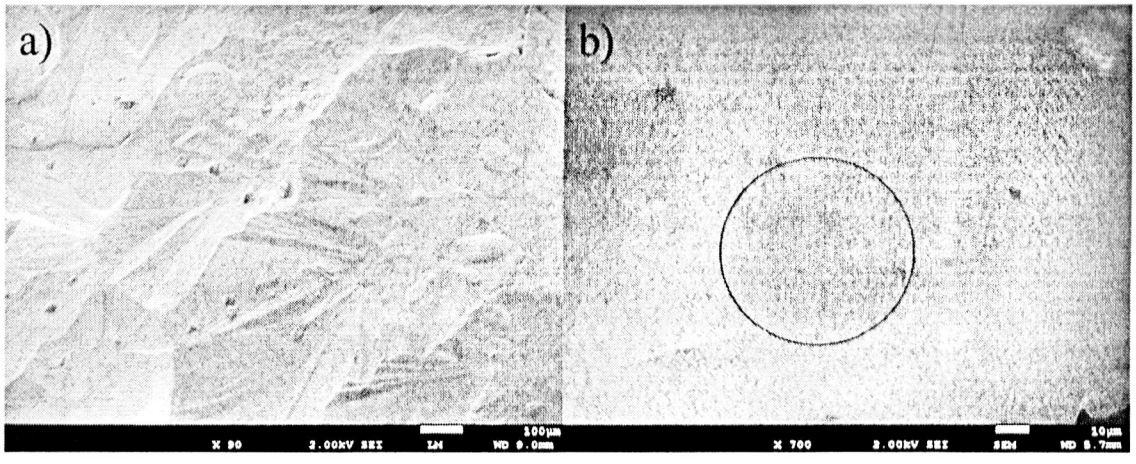

Figure 26 SEM images of fabricated single layer at a) low magnification b) high magnification

4.4 Fabrication of 3D ceramic blocks

In spite of using laser scanning parameters identified via the previous experiments, the test using laser 1 was not able to fabricate any coherent ceramic blocks. Laser 1 is an ytterbium or Nd:YAG fiber laser (λ = 1.07 μm) of Gaussian distribution with maximum laser power of 400W and laser beam diameter of 80μm. Figure 27 shows some of the results of the laser scanning of alumina-zirconia powder and their corresponding scanning parameters.

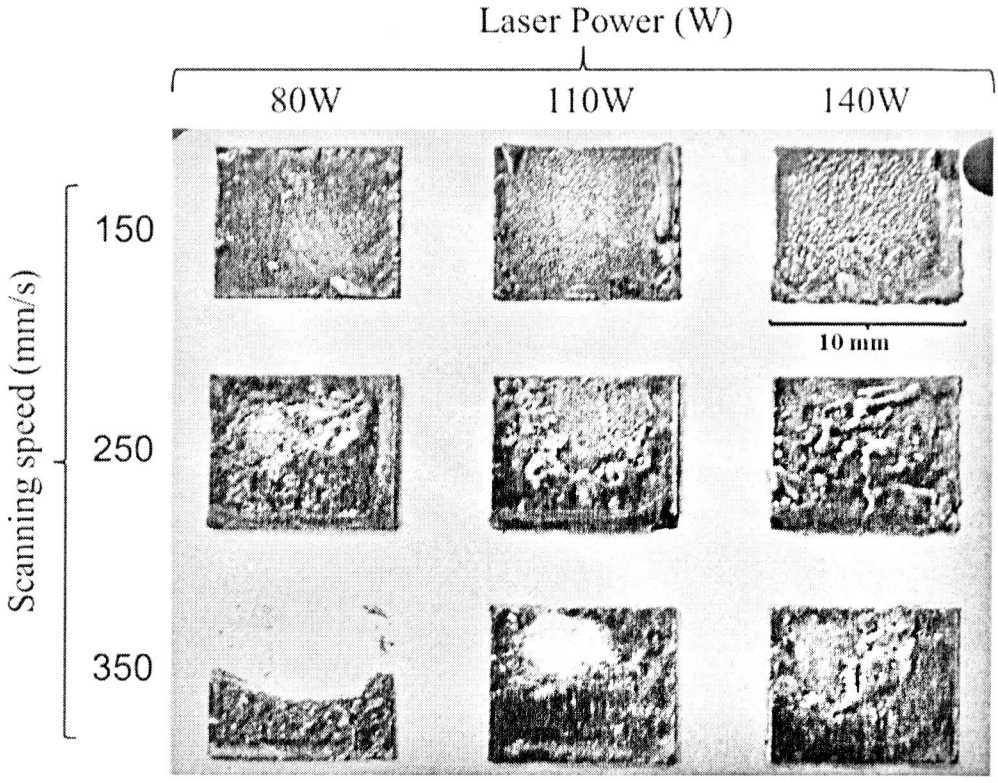

Figure 27 Multilayer SLM parts using laser 1

In 3D fabrication, the additional parameter is the layer thickness. In this work, the layer thickness was set on 100 μm for this experiment. The scanning orientation for each layer is shown in Figure 28. In each layer the scanning direction is rotated 45°. This randomizes and minuses the residual stress direction experienced by the final product.

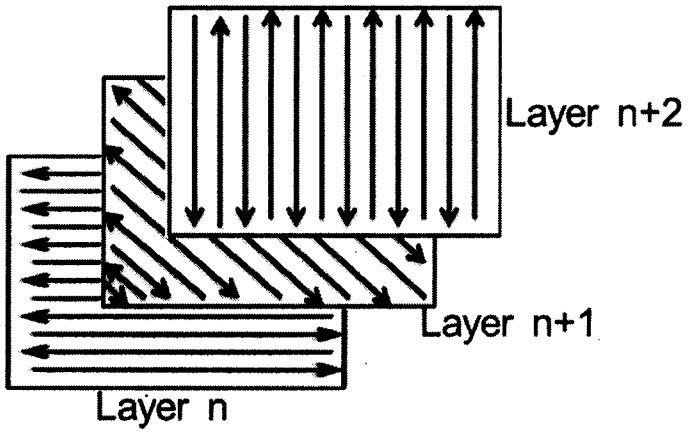

Figure 28 scanning orientation in multilayer fabrication

The main reason for not being able to form a coherent solid ceramic block with this laser is due to the high transmittance of laser energy through ceramic powder. As a result, the intensity of the laser received by some of the powder particles in the second and third layers would be much higher. This cause intensive light during scanning was shown in Figure 29. This implies that laser penetration and resolution control in laser melting of ceramic powder with laser 1 is complicated.

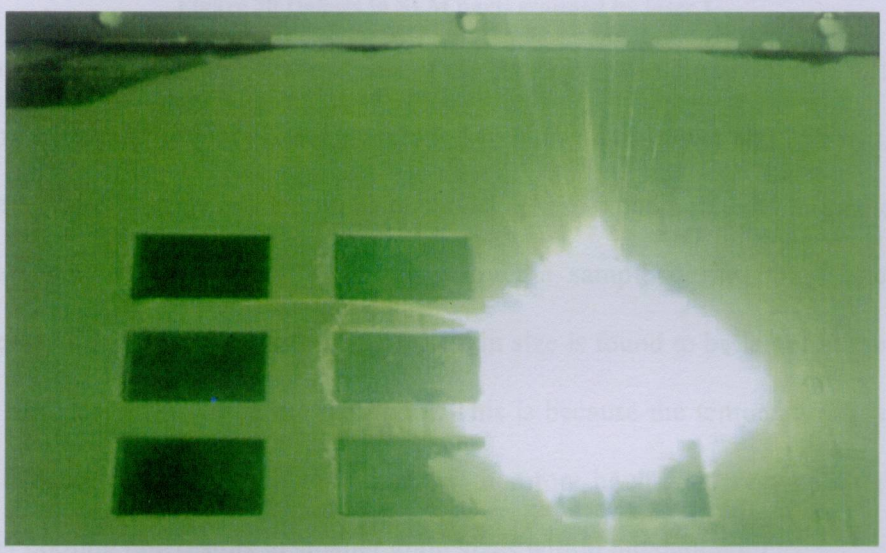

Figure 29 Intensive lights during laser scanning

In addition, it was observed that at combinations of high laser power and low scanning speed, some of the ceramic powders were 'pushed' off from the powder bed. The phenomenon occurs due to momentum transfer by laser. Defects in the fabricated SLM parts are shown in Figure 30. As laser beam diameter in laser1 (80 μm) is much smaller than laser 2 (730 μm), the push off phenomenon is more serious in the experiments by laser 1.

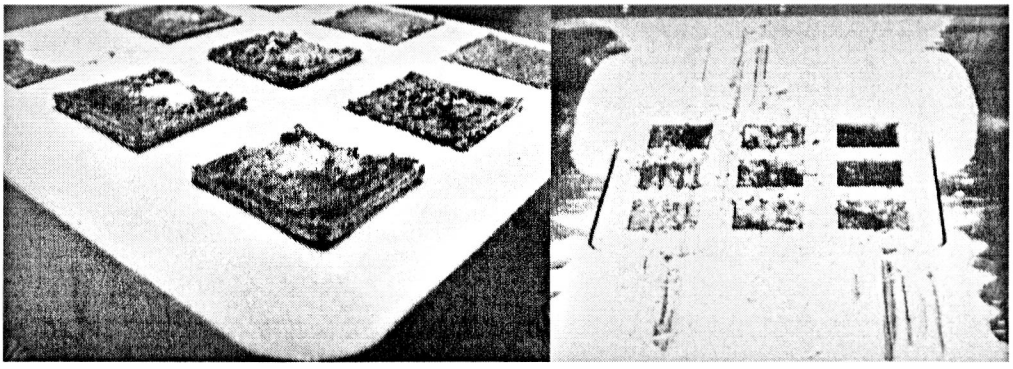

Figure 30 Defects in SLM parts scanned by laser 1

Figure 31 illustrates the SEM pictures of the fabricated sample under two different magnifications. The process parameters is 140W for laser power and 250 mm/s for scanning speed. Many cracks can be observed. These could be due to large thermal gradient and thermal shock experienced by the sample during the fabrication process. At the higher magnification, the grain size is found to be larger at the melt pool boundary than within the melt pool. This is because the temperature gradient is within the melt pool than the boundary therefore having a larger cooling rate. Larger cooling rate results in smaller grain sizes within the melt pool.

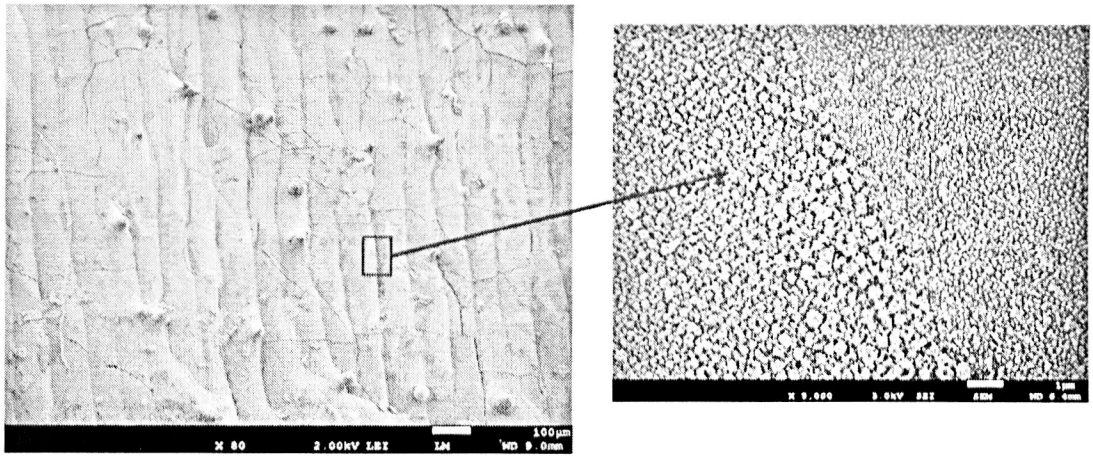

Figure 31 SEM pictures of alumina zirconia sample fabricated by SLM using laser 1

The second laser beam module in the SLM 250HL machine used in this experiment is a uniformly distributed Nd:YAG laser beam of spot size diameter 760 um and maximum power of 1000 W. As the second laser beam is uniformly distributed, the energy is constant with the laser beam radius.

Figure 32 shows the samples fabricated under varying laser powers between 700 W to 900 W at 100 W interval and scanning speeds of 400 mm/s and 500 mm/s. These ranges are selected based on the energy density required to melt the ceramic mixture. The energy density in these samples varies from 1.9 J/mm^2 to 3.1 J/mm^2.

The scanning strategy used with the second laser beam is the same as previously mentioned with laser 1 use scanning direction rotates 45° in each layer.

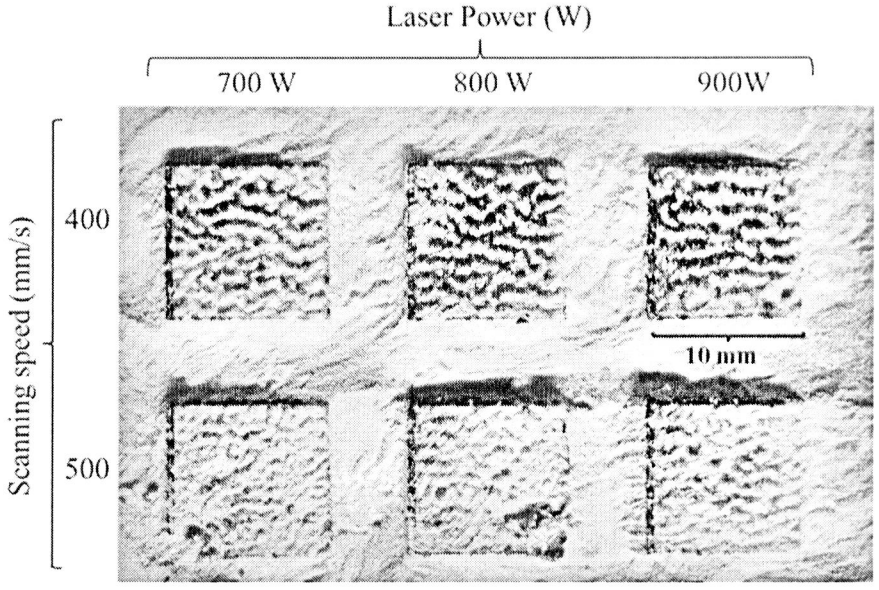

Figure 32 Alumina-zirconia SLM parts using Laser2

Figure 33 shows the blocks built under the process window mentioned above with a 500 μm layer thickness. This large layer thickness was chosen as it was observed

previously, most of the powder were expelled and burnt out from the powder bed under the process parameters used with first laser beam. The energy density required to melt the alumina-zirconia powder mixture is so high that the recoil pressure generated during the scanning process sputtered the powder particles away from the powder bed. It was not possible to further reduce the energy density in order to avoid powder expulsion as it will result in little or no melting. The final height of the blocks built under the second laser beam is 5 mm with a total of 10 layers.

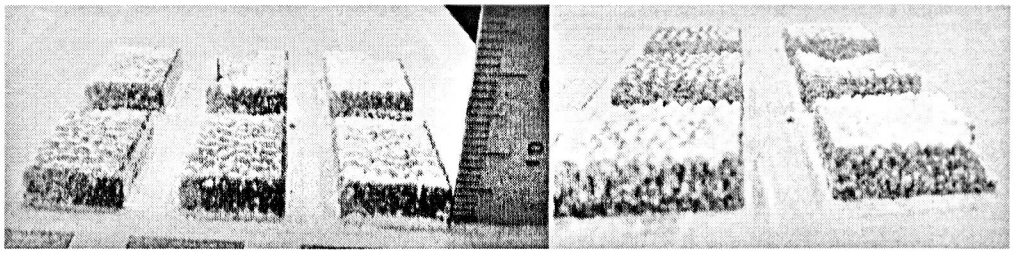

Figure 33 Fabricated alumina-zirconia 3D parts using laser 2

Figure 34 shows the SEM pictures of the samples fabricated under the second laser beam at different magnifications. As compared to the surface morphology of the samples fabricated under the first laser beam, the sizes of the solidified melt tracks are much larger. This is because the laser beam diameter of the second laser beam is about 9 times the size of the first laser beam. Thus, a larger melt pool is formed and solidified as observed from the SEM images. Also it can be observed that the samples fabricated under laser 2 are more porous. From the surface morphology, in higher magnification image, no micro cracks are observed in these samples unlike those fabricated in laser 1 due to the low temperature gradient experienced by the material across beam diameter under laser 2.

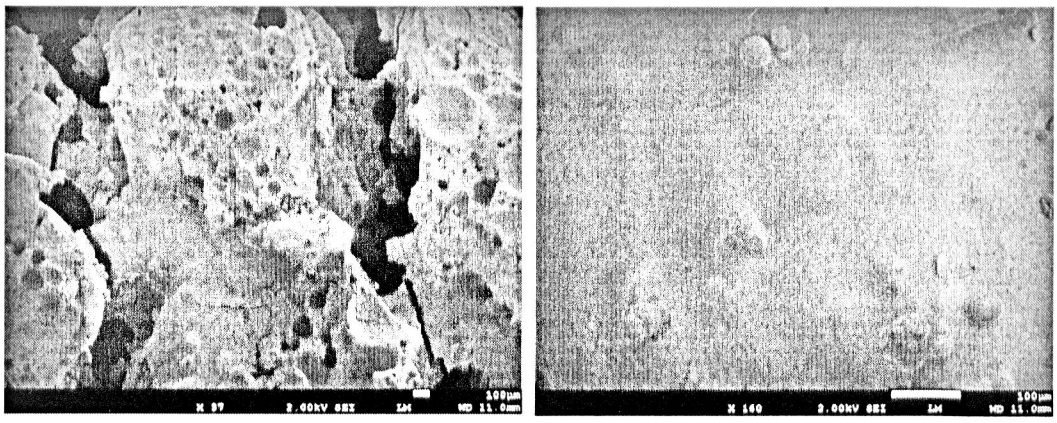

Figure 34 SEM pictures of alumina-zirconia SLM parts in ×37 and × 160 magnifications respectfully

Figure 35 shows the SEM pictures of the samples fabricated under laser 2 at higher magnifications. The microstrcutures are observed to be flake-shaped due to the diffrences in surface tension between alumina and zirconia individually.

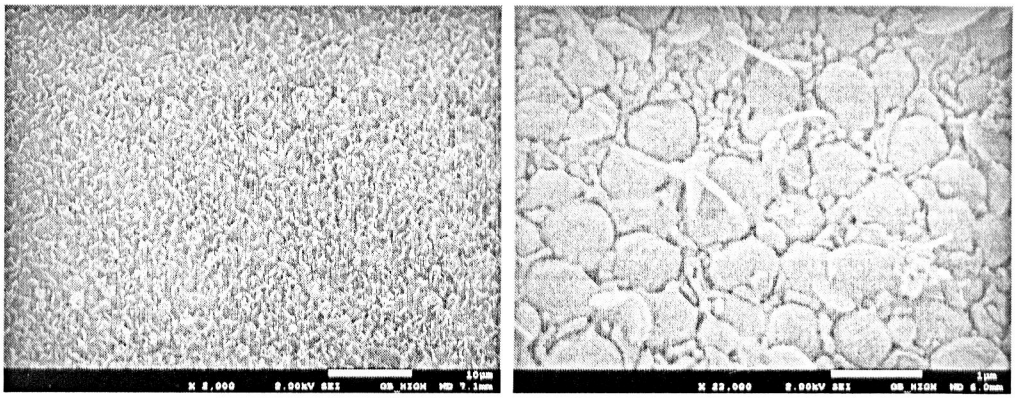

Figure 35 SEM pictures of alumina-zirconia SLM parts in ×2000 and × 22000 magnifications respectfully

The table below shows the density results for parts fabricated under the second laser beam. It can be observed that the density is higher at high laser power and lower at low scan speed. This is because more energy is deposited with increased laser power and reduced scan speed to fully melt the ceramic mixture. However, as the laser power of the second laser beam is limited to 1000 W, the upper limit of the experiments was set at 900 W to avoid fluctuations and inaccuracy occurring at the 1000 W limit.

Table 6 Density measurment results for fabricated alumina-zirconia 3D parts via laser 2

Laser power / Scanning speed	700 W	800 W	900 W
400 mm/s	62.33%	65.04%	69.41%
500 mm/s	55.30%	60.56%	68.35%

The density is measured via the Archimedes principle using equation number (1).

Percentage of density is calculated using the equation below.

$$\%Density = \frac{D_s}{D_{Alumina-Zirconia}} \times 100\% \quad (4)$$

D_s = Density of the sample

$D_{Alumina\text{-}Zirconia}$ = Density Alumina-Zirconia (5.4725 g/mm^3)

The composition of the SLM fabricated alumina-zirconia parts were verified by SEM-EDX and XRD. Figure 36 illustrates the EDX result of SLM fabricated ceramic part. XRD results of the alumina-zirconia powder and 3D fabricated parts are shown in Figure 37. The only three elements detected in EDX results are oxygen, aluminum and zirconium which mean the SLM fabricated parts are not contaminated during the melting and solidification in SLM process.

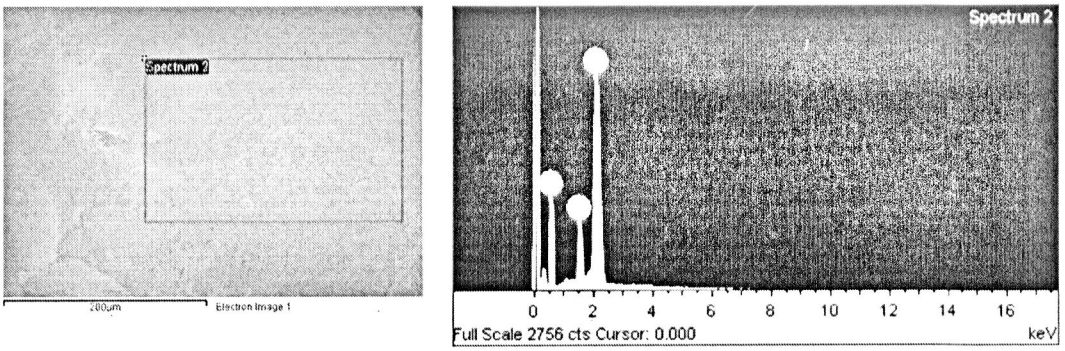

Element	Weight%	Atomic%
O K	47.26	80.61
Al K	5.06	5.12
Zr L	47.68	14.26
Totals	100.00	

Figure 36 EDX results of SLM alumina-zirconia 3D parts

The phase composition in the XRD result features a high degree of crystallinity dominated by the metastable tetragonal-ZrO_2 and Al_2O_3 phases. In the presence of yttrium oxide Y_2O_3 in Zirconia powder (3YSZ), the monoclinic-ZrO_2 turned into metastable tetragonal-ZrO_2 during melting and solidification process. On the other hand, the metastable tetragonal-ZrO_2 is stabilized by constraining Al_2O_3 matrix. As a matter of fact the ZrO_2-Al_2O_3 bulk composite is a classical model of transformation-toughening ceramic system. The toughening influence is usually expressed as an alumina matrix employs local compressive stresses around small zirconia crystals. In this situation transformation from tetragonal to monoclinic ZrO_2 is obstructed. And metastable tetragonal-ZrO_2 is the only zirconia phase in the SLM fabricated parts.

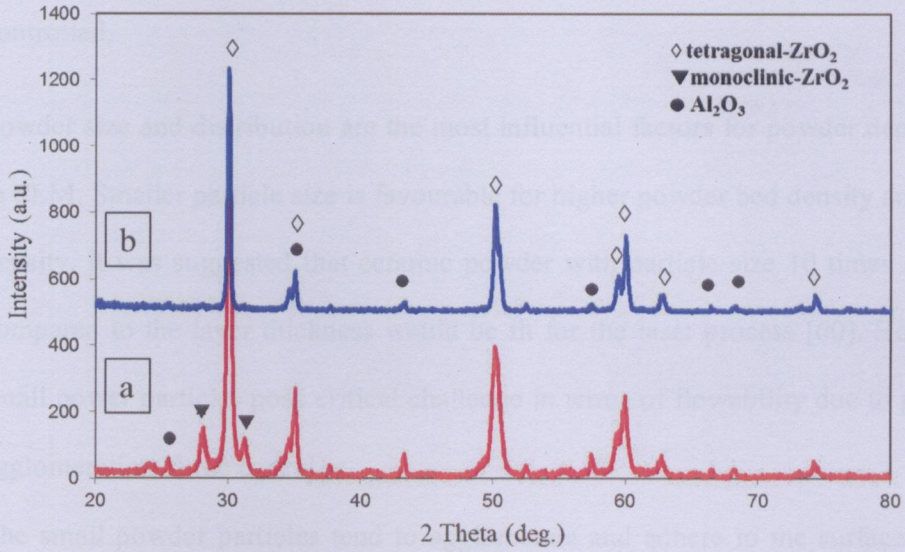

Figure 37 XRD result of alumina-zirconia a) powder b) 3D part

4.5 Challenges and difficulties

This section presents technical issues during SLM processing of ceramic powder, including power layer deposition, laser-powder interaction, melting and consolidation mechanism and residual stress analysis, where further research is needed.

4.5.1 Powder layer deposition

The SLM system uses a blade to spread powder onto the substrate platform or the preceding part. To form a thin and even powder layer, good flowability of powder particles is necessary [83]. Powder bed density also has a direct influence on the final part quality. Powder parameters such as particle size and distribution,

particle shape and flow characteristics are important and have to be well-controlled.

Powder size and distribution are the most influential factors for powder deposition in SLM. Smaller particle size is favourable for higher powder bed density and solid density. It was suggested that ceramic powder with particle size 10 times smaller compared to the layer thickness would be fit for the laser process [60]. However, small power particles pose critical challenge in terms of flowability due to powder agglomeration in the cartridge.

The small powder particles tend to agglomerate and adhere to the surface of the coater and printing platform due to electrostatic charge. This created challenge in achieving a homogeneous powder layer deposition. Removing smaller particles from the powder feedstock may improve the flowability but will negatively impact the density of the powder-bed and subsequently the fabricated part [84]. Spierings et al. has given some suggestions on metallic powder size distribution selection for SLM process [84]. Similar research on ceramic powder size distribution is also needed.

Powder shape has an influence on the powder spreading and layer density of the powder bed [85]. Wilkes et al. also informed that particle shape has a strong influence on the density of ceramic object produced by SLM. The improvement in density of SLM parts was thought to be related to the spherical powder shape [86]. As there is no ceramic powder products specially designed for SLM process, it may not be easy to select the optimal powder for SLM machine. Different powder types such as crushed and atomized are commercially available. Ceramic powder

produced by crushing method has an angular shape and relatively high bulk density, which is widely used in the industry. Spherical particles atomized by spray drying technology from fine primary ceramic particles (<1μm) to tens of microns particle have a better flow ability compared with crushed products [87].

Powder flowability measurement is necessary in SLM process for quantitative prediction of the powder deposition behaviour. Common methods for measuring powder character include angle of repose, bulk density, tapped density, Carr's compressibility index and Hausner ratios, which are mainly for specific processes such as compaction, storage and volume filling [81, 88]. Thus, it is desirable to measure flowability at flow conditions that are representative of SLM processing situations. Further research is needed to develop a powder performance index tailored to SLM processing of ceramic.

4.5.2 Laser-powder interaction

The SLM process uses Nd:YAG laser or fibre laser with wavelengths of approximately 1.06 μm as a heat source, which allows for more efficient energy focusing to melt the powder as compared to CO2 laser with wavelengths of 10.6μm. This would be suitable for ceramics, especially for oxide ceramic with high melting temperature. A major challenge in the processing of oxide ceramic with a near infrared wavelength laser is related to their low and temperature dependent absorbance of the laser wavelength, as described by Fermi function [29, 89]. The experimental absorbance measurement of ceramic powder is shown in Table 7 [90]. The absorption rate of oxide powders to laser with 1.06μm

wavelength is less than 10%, which causes high laser energy loss and reduces production rate.

Table 7Absorptance (A) of ceramic powder measured with two lasers: Nd:YAG(λ=1.06μm) and CO2(λ=10.6μm) [90]

Material	A	
	λ=1.06μm	λ=10.6μm
Al2O3	3%	96%
SiO2	4%	96%
SiC	78%	66%
WC	82%	48%

A Q-switched laser system has been developed for micro sintering of ceramic [29, 91]. The Q-switched pulse laser would be more suitable for ceramic process as the high energy laser pulses could increase the frequency of multi-photon excitation of electrons in the valence band and result in higher absorption rate. High density ceramic parts of several millimetres high, as well as metal parts, have been made by the pulsed laser system [28, 92, 93]. However, the recoil effect of heated vapour induced by higher energy pulse would influence the stability of the powder bed and melt pool, as well as the parts qualities.

Optical interaction of laser with the powder could also impact the laser beam propagation profile in the powder bed. The powder bed in SLM machine has a high porosity as powder is spread freely without compression or heat treatment on the platform. The input laser beam under-goes multiple scattering or reflections in the

bulk powder layer before it is being absorbed to generate the corresponding powder density and layer thickness [94, 95]. Liu et al modelled the laser beam propagation of fibre laser through silica powder. In their model, it was noticed that the laser beam was further focused into the powder bed by the spherical geometry of the silica powder. Energy absorbed was not uniform with the maximum absorption areas occurring near to the third layer of the powder stacking [96]. Streek et al. used ray tracing algorithm to describe the laser energy absorption and conversion during laser sintering process, which could be regarded as a function of grain size, grain density, laser beam intensity and material properties [97]. It was reported that powder particles with small size also require increased laser energy penetration to form melting pool due to their high surface-to-volume ratio [98].

4.5.3 Melting and consolidation mechanism

For partial melting process, the laser radiation focused to melt the grains surface or particles with low melting point. The molten materials act as a binder to form necks connection between particles and subsequently form a 3D porous structure after laser process [99]. The temperature effects, gravity and capillary forces are the main driving forces for consolidation of molten material during partial melting. For full melting, moving molten pool is formed in respond to the moving laser energy input. The interaction between laser and powder induces high temperature gradients and significant temperature differences inside the small molten pool as the melt pool experienced high cooling rates at the passing of laser scanning [100]. The temperature gradients can cause rapid motion, known as Marangoni flow. This effect becomes increasingly significant for ceramics as ceramics have higher

melting point and lower thermal conductivity compared with metallic materials. Similar phenomenon could be seen during other laser-ceramic process such as laser welding of aluminium and alumina. The energy transport was more obvious for alumina compared with aluminium [101].

During SLS/SLM process, three types of process behavior can be observed, namely, formation of irregular and unstable melt tracks caused by lack of melting, continuous and stable melt tracks and balling effect. These behaviors are influenced by powder characters and process parameters such as laser power, scanning speed and layer thickness [99, 102]. Balling effect occurs due to poor wettability between the molten pool and underlying solid, causing the molten pool to breakup into small ceramic spheres [103]. As for laser processing of ceramics, the poor wetting behavior of the liquid phase would lead to formation of loose droplets and inhomogeneous layer surface quality.

Modelling work on temperature and stress profiles using various parameters during laser processing ceramic materials has been reported. Li et al. developed a volumetric heating source model for laser surface melting ceramics [104]. However, fluid flow should be added into their models for large molten pool. Tian et al. investigated the effect of different laser scan patterns in laser direct sintering ceramics [105]. Further study on simulating the SLM process of ceramic is required for parameter selection and optimization.

4.5.4 Thermal and residual stress analysis

The thermal effect in full melting process via laser would generate significant residual stress and strain during rapid solidification. In the case of partial melting without infiltration, the residual stresses were also reported [106]. The residual stress depends on the temperature gradient and material physical properties. The ceramic materials are generally considered to be of low plastic deformation, with typical elongation at break of oxide ceramic at about 0.2% to 0.6% [107].

Rapid melting and cooling of ceramics in SLM also will negatively impact the grain size of the ceramic part produced. Conventionally, ceramics are sintered using solid state sintering methods in which slow diffusion of atoms are needed to achieve fine grain size. This low sintering temperature will also help to maintain the fine grain size, which is the key characteristic for high mechanical properties of high performance ceramics. However the laser will not be able to provide such capacity for slow diffusion and as a result, the high temperature gradient will generate a lot of cracks in the ceramic part.

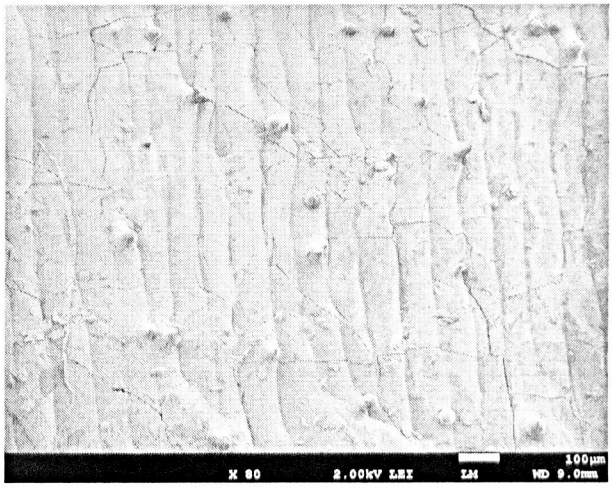

Figure 38 top surface SEM image of zirconia/alumina part

Fig.38 shows the top surface SEM image of zirconia/alumina part built by SLM, highly dense surface as well as cracks can be observed. Li et al. found that for laser-ceramic interaction process, the whole laser melted track is in tension, and crack occurs in the region of highest tensile stress throughout the solidified ceramic tracks created by laser surface melting [108]. Heat treatment can be applied in the laser process to reduce the temperature gradients, as well as thermal stress. A higher base platform heating temperature will be needed for ceramic materials compared to metal. Meanwhile, a specific type of ceramic has shown the characteristic of superplasticity with exceptionally large elongation in tensile deformation at high temperature [109]. This property would reduce the cracking tendency of laser treated ceramic parts. Hagedorn et al. used preheating setup during the process, reaching temperature >1400°C to build highly dense and crack-free parts. The problems of this solution include rough surface and poor contour precision due to large melt pool and powder sintering with high-temperature preheating. Other approaches to reduce the residual stress focus on investigation of processing factors such as sample height, exposure strategy and the use of pulse laser [106, 110].

Chapter 5: Conclusions and Future work

5.1 Conclusions:

As powder flowability is one of the important issues in the SLM process, Spray drying was conducted to improve the flowability of alumina and zirconia mixture powder. It was observed that no phase change occurred after the spray drying process. Fine particles size (< 5 μm) granulated into larger particles size (< 50 μm) after spray drying. The improvement in powder flowability was further proven by a dynamic powder characterisation methodology. Understanding of powder particle size distribution and shape helps to estimate the powder flow behaviour under different processing conditions especially SLM process. For this aim the dynamic behaviour of Al_2O_3- ZrO_2 ceramic powders were characterized under a revolutionary condition by a system called Revolution Powder Analyzer. Results showed that spherical particle shape powders with larger particle size, narrower particle size distribution and smoother particles surface show better flowability. On the other hand, powder with a wider particle size distribution provides more packed and even layer during SLM process.

The series of experiments were tested on the spray dried mixture powder. The experiments were conducted three stages. Single-track, single-layer and 3D blocks fabrication (multilayers). The results showed that the SLM machine is capable of melting ceramic powders with high melting point. Different scanning parameters were tested to optimise parameters including laser power, scanning speed and hatch spacing. Finally, multilayer or ceramic 3D blocks were experimented via SLM

machine. A combination of high laser power and low scanning speed was required to form the ceramic powder into a coherent structure. However, the density of the fabricated 3D parts was low and the parts were also fragile and unstable. These results showed that with current state of technology, it is still a challenge to directly fabricate dense ceramic components using SLM. Following the insights obtained from these experiments, the critical challenges of this project were identified and discussed, including ceramic powder layer deposition, laser-powder particles interaction, the dynamic melting and consolidation mechanism, process parameter optimisation and residual stress analysis of the ceramic materials processed with SLM.

5.2 Future work:

Successful integration of ceramic into selective laser melting technology will induce significance development in the field of technical ceramics application. Further research on the technical issues and challenges of the SLM process of ceramic powder are required, specifically in resolving the challenges in powder deposition, laser-powder bed interaction, melting and consolidation mechanism, process parameters optimization and residual stress analysis.

A possible step for further research is material selection. Taking advantage of ceramic composite properties is useful to resolve some of challenges in using the SLM process for ceramic materials.

References:

1. Chua, C.K., K.F. Leong, and C.C.S. Lim, *Rapid prototyping: principles and applications*. 2010: World Scientific Publishing Company.

2. Hench, L.L. and G.Y. Onoda, *Ceramic processing before firing*. 1978, New York: Wiley. 512.

3. Fries, R. and B. Rand, *Slip-Casting and Filter-Pressing*, in *Materials Science and Technology*. 2006, Wiley-VCH Verlag GmbH & Co. KGaA.

4. Zauner, R., *Micro powder injection moulding*. Microelectronic Engineering, 2006. 83(4–9): p. 1442-1444.

5. Su, B., S. Dhara, and L. Wang, *Green ceramic machining: A top-down approach for the rapid fabrication of complex-shaped ceramics*. Journal of the European Ceramic Society, 2008. 28(11): p. 2109-2115.

6. Filser, F., P. Kocher, and L. Gauckler, *Net-shaping of ceramic components by direct ceramic machining*. Assembly Automation, 2003. 23(4): p. 382-390.

7. Krell, A., et al., *Processing of High - Density Submicrometer Al2O3 for New Applications*. Journal of the American Ceramic Society, 2003. 86(4): p. 546-53.

8. Sachs, E.M., et al., *Three-dimensional printing techniques*. 1993, Google Patents.

9. Cima, M., et al. *Slurry-based 3DP and fine ceramic components*. in *Proceedings of Solid Freeform Fabrication Symposium, Austin, TX, USA*. 2001. ISTE USA.

10. Wang, H.-R., *Gradient-Index (GRIN) lenses by Slurry-based Three-Dimensional Printing (S-3DP)*. 2005, Massachusetts Institute of Technology.

11. Edirisinghe, M.J., *Solid freeform fabrication methods for engineering ceramics*. British ceramic transactions, 1998. 97(6): p. 283-286.

12. Evans, J.R., M.J. Edirisinghe, and J.H. Song, *Direct Ink - Jet Printing of Vertical Walls*. Journal of the American Ceramic Society, 2002. 85(8): p. 2113-2115.

13. Zhao, X., et al., *Ink-jet printing of ceramic pillar arrays*. Journal of materials science, 2002. 37(10): p. 1987-1992.

14. Zhao, X., et al., *Formulation of a ceramic ink for a wide-array drop-on-demand ink-jet printer*. Ceramics International, 2003. 29(8): p. 887-892.

15. Onagoruwa, S., S. Bose, and A. Bandyopadhyay, *Fused deposition of ceramics (FDC) and composites*. School of Mechanical and Materials Engineering Washington State University Pullman, WA, 2001: p. 99164-2920.

16. Zhang, Y., et al., *Al2O3 ceramics preparation by LOM (laminated object manufacturing)*. The International Journal of Advanced Manufacturing Technology, 2001. 17(7): p. 531-534.

17. Weisensel, L., et al., *Laminated object manufacturing (LOM) of SiSiC composites.* Advanced Engineering Materials, 2004. 6(11): p. 899-903.

18. Bertsch, A., S. Jiguet, and P. Renaud, *Microfabrication of ceramic components by microstereolithography.* Journal of micromechanics and microengineering, 2004. 14(2): p. 197.

19. Chartier, T., et al., *Stereolithography of structural complex ceramic parts.* Journal of Materials Science, 2002. 37(15): p. 3141-3147.

20. Halloran, J.W., *Freeform fabrication of ceramics.* British ceramic transactions, 1999. 98(6): p. 299-303.

21. Savalani, M., et al., *Fabrication of porous bioactive structures using the selective laser sintering technique.* Proceedings of the Institution of Mechanical Engineers, Part H: Journal of Engineering in Medicine, 2007. 221(8): p. 873-886.

22. Lee, I., A. Manthiram, and H. Marcus. *Selective Laser Sintering of Alumina-Zinc Borosilicate Glass Composites using Monoclinic HB02 as a Binder.* in *Proceedings to the Solid Freeform Fabrication Symposium*. 1995.

23. Fischer, H., et al., *Bone substitute implants made of TCP/Glass composites using selective laser melting technique, RWTH Aachen University.* Fraunhofer Institute for Laser Technology ILT, Ber DKG, 2006. 83: p. 57-60.

24. Shishkovsky, I., et al., *Alumina–zirconium ceramics synthesis by selective laser sintering/melting.* Applied Surface Science, 2007. 254(4): p. 966-970.

25. Bertrand, P., et al., *Ceramic components manufacturing by selective laser sintering.* Applied Surface Science, 2007. 254(4): p. 989-992.

26. Tang, H.-H., M.-L. Chiu, and H.-C. Yen, *Slurry-based selective laser sintering of polymer-coated ceramic powders to fabricate high strength alumina parts.* Journal of the European Ceramic Society, 2011. 31(8): p. 1383-1388.

27. Klocke, F., et al., *Investigations on laser sintering of ceramic slurries.* Production Engineering, 2007. 1(3): p. 279-284.

28. Exner, H., et al., *Laser micro sintering: A new method to generate metal and ceramic parts of high resolution with sub-micrometer powder.* Virtual and physical prototyping, 2008. 3(1): p. 3-11.

29. Regenfuss, P., et al., *Principles of laser micro sintering.* Rapid Prototyping Journal, 2007. 13(4): p. 204-212.

30. Sun, M.L., L. Lu, and J.Y.H. Fuh, *Microstructure and properties of Fe-base alloy fabricated using selective laser melting,* in *Second International Symposium on Laser Precision Microfabrication*, I. Miyamoto, et al., Editors. 2002, Spie-Int Soc Optical Engineering: Bellingham. p. 139-142.

31. Santos, E., et al., *Fabrication of titanium dental implants by selective laser melting*, in *Fifth International Symposium on Laser Precision Microfabrication*, I. Miyamoto, et al., Editors. 2004, Spie-Int Soc Optical Engineering: Bellingham. p. 268-273.

32. Savalani, M.M., et al., *Selective Laser Melting of Aluminum and its alloys*, in *NZ Rapid Product Development Conference*. 2011: Auckland, New Zealand.

33. Kempen, K., et al., *Mechanical properties of AlSi10Mg produced by Selective Laser Melting*. Physics Procedia, 2012. 39: p. 439-446.

34. Wu, W., Y. Yang, and Y. Huang, *Direct manufacturing of Cu-based alloy parts by selective laser melting*. Chin. Opt. Lett., 2007. 5(1): p. 37-40.

35. Amato, K.N., et al., *Microstructures and mechanical behavior of Inconel 718 fabricated by selective laser melting*. Acta Materialia, 2012. 60(5): p. 2229-2239.

36. Ng, C.C., et al., *Microstructure and mechanical properties of selective laser melted magnesium*. Applied Surface Science, 2011. 257(17): p. 7447-7454.

37. Deprez, K., et al., *Rapid additive manufacturing of MR compatible multipinhole collimators with selective laser melting of tungsten powder.* Medical Physics, 2013. 40(1).

38. Xin, X.Z., et al., *Corrosion characteristics of a selective laser melted Co-Cr dental alloy under physiological conditions.* Journal of Materials Science, 2012. 47(12): p. 4813-4820.

39. Khan, M. and P. Dickens, *Selective laser melting (SLM) of gold (Au).* Rapid Prototyping Journal, 2012. 18(1): p. 81-94.

40. Yadroitsev, I., P. Bertrand, and I. Smurov, *Parametric analysis of the selective laser melting process.* Applied Surface Science, 2007. 253(19): p. 8064-8069.

41. Yasa, E., et al. *Investigation of sectoral scanning in selective laser melting*. in *Biennial ASME Conference on Engineering Systems, Design and Analysis*. 2010. Istanbul, Turkey.

42. Dadbakhsh, S., L. Hao, and N. Sewell, *Effect of selective laser melting layout on the quality of stainless steel parts*. Rapid Prototyping Journal, 2012. 18(3): p. 241-249.

43. Ghany, K.A. and S.F. Moustafa, *Comparison between the products of four RPM systems for metals.* Rapid Prototyping Journal, 2006. 12(2): p. 86-94.

44. Greenemeier, L. *NASA Plans for 3-D Printing Rocket Engine Parts Could Boost Larger Manufacturing Trend*. Scientific American 2012 [cited 2013 29 July]; Available from: http://www.scientificamerican.com/article.cfm?id=nasa-3-d-printing-sls-rocket-engine&WT.mc_id=SA_CAT_TECH_20121113.

45. Gasser, A., et al., *Laser Metal Deposition and SLM in Turbo-Engine Applications.* Laser Technik Journal, 2010. 7(2): p. 58 - 63.

46. Vilaro, T., S. Abed, and W. Knapp. *Direct manufacturing of technical parts using selective laser melting: example of automotive application.* in *Proc. of 12th European Forum on Rapid Prototyping*. 2008.

47. Lu, L., et al., *In situ formation of TiC composite using selective laser melting.* Materials Research Bulletin, 2000. 35: p. 1555 - 1561.

48. Gill, T. and B. Hon. *Selective laser sintering of SiC-polyamide matrix composites.* in *Solid Freeform Fabrication Symposium*. 2002. Austin, Texas, USA.

49. Hon, K.K.B. and T.J. Gill, *Selective Laser Sintering of SiC/Polyamide Composites.* CIRP Annals - Manufacturing Technology, 2003. 52(1): p. 173-176.

50. Gu, D., et al., *Bulk-form TiCx/Ti nanocomposites with controlled nanostructure prepared by a new method: selective laser melting.* Journal of Physics D: Applied Physics, 2010. 43(29): p. 295402.

51. Biedunkiewicz, A., et al., *Preparation of stainless steel-TiC composite by selective laser melting.* Chemické Listy, 2011. 105: p. 773 - 774.

52. Gu, D., et al., *Selective Laser Melting of in-situ TiC/Ti5Si3 composites with novel reinforcement architecture and elevated performance.* Surface and Coatings Technology, 2011. 205(10): p. 3285-3292.

53. Mumtaz, K.A. and N. Hopkinson, *Laser melting functionally graded composition of Waspaloy® and Zirconia powders.* Journal of Materials Science, 2007. 42(18): p. 7647-7656.

54. Hao, L., et al., *Selective laser melting of a stainless steel and hydroxyapatite composite for load-bearing implant development.* Journal of Materials Processing Technology, 2009. 209(17): p. 5793-5801.

55. Lindner, M., et al., *Manufacturing of individual biodegradable bone substitute implants using selective laser melting technique.* J Biomed Mater Res A, 2011. 97(4): p. 466-71.

56. Shishkovskii, I.V., I.A. Yadroitsev, and I.Y. Smurov, *Selective laser sintering/melting of nitinol-hydroxyapatite composite for medical applications.* Powder Metallurgy and Metal Ceramics, 2011. 50: p. 275 - 283.

57. Dadbakhsh, S. and L. Hao, *In Situ Formation of Particle Reinforced Al Matrix Composite by Selective Laser Melting of Al/Fe2O3 Powder Mixture.* Advanced Engineering Materials, 2012. 14(1-2): p. 45-48.

58. Tay, B.Y., J.R.G. Evans, and M.J. Edirisinghe, *Solid freeform fabrication of ceramics.* International Materials Reviews, 2003. 48(6): p. 341-370.

59. Wilkes, J. and K. Wissenbach, *Rapid Manufacturign of Ceramic Components for Medical and Technical Applications via Seletive Laser Melting*. 2006, Fraunhofer Institute for Laser Technology ITL. p. 6.

60. Bertrand, P., et al., *Ceramic components manufacturing by selective laser sintering.* Applied Surface Science, 2007. 254(4): p. 989-992.

61. Hagedorn, Y.-C., et al., *Net shaped high performance oxide ceramic parts by selective laser melting.* Physics Procedia, 2010. 5: p. 587-594.

62. Hagedorn, Y.C., et al. *SLM of net-shaped high strength ceramics: new opportunities for producing dental restorations.* in *SFF Symposium*. 2011. Austin, Texas, USA.

63. Tang, Y., et al., *Direct laser sintering of a silica sand.* Materials and Design, 2003. 24: p. 623 - 629.

64. Liu, F.-H., *Synthesis of bioceramic scaffolds for bone tissue engineering by rapid prototyping technique.* Journal of Sol-Gel Science and Technology, 2012. 64(3): p. 704-710.

65. Tian, X., et al., *Scan pattern, stress and mechanical strength of laser directly sintered ceramics.* The International Journal of Advanced Manufacturing Technology, 2012. 64(1-4): p. 239-246.

66. Sasaki, H., et al., *HIGH-POWER-DENSITY-SOLID-OXIDE-ELECTROLYTE FUEL-CELLS.* Journal of the Electrochemical Society, 1992. 139(1): p. L12-L13.

67. Shao, Z. and S.M. Haile, *A high-performance cathode for the next generation of solid-oxide fuel cells.* Nature, 2004. 431(7005): p. 170-173.

68. Reim, M., et al., *Silica aerogel granulate material for thermal insulation and daylighting.* Solar Energy, 2005. 79(2): p. 131-139.

69. NASA, *Orbiter Thermal Protection System*, in *NASA Facts*, N.A.a.S. Administration, Editor. 2006.

70. Hagedorn, Y., et al. *SLM of net-shaped high strength ceramics: new opportunities for producing dental restorations.* in *Proceedings of the Solid Freeform Fabrication Symposium*. 2011.

71. Rizkalla, A. and D. Jones, *Mechanical properties of commercial high strength ceramic core materials.* Dental materials, 2004. 20(2): p. 207-212.

72. Rizkalla, A.S. and D.W. Jones, *Indentation fracture toughness and dynamic elastic moduli for commercial feldspathic dental porcelain materials.* Dental Materials, 2004. 20(2): p. 198-206.

73. Ho, G.W. and J.P. Matinlinna, *Insights on ceramics as dental materials. Part I: ceramic material types in dentistry.* Silicon, 2011. 3(3): p. 109-115.

74. Kelly, J.R., I. Nishimura, and S.D. Campbell, *Ceramics in dentistry: Historical roots and current perspectives.* The Journal of Prosthetic Dentistry, 1996. 75(1): p. 18-32.

75. Cawley, J.D. and W.E. Lee, *Oxide ceramics.* Materials Science and Technology, 1994.

76. Kelly, J.R. and I. Denry, *Stabilized zirconia as a structural ceramic: an overview.* Dental materials, 2008. 24(3): p. 289-298.

77. Schulz, B., *High temperature thermal conductivity of irradiated and non-irradiated α-Al2O3.* Journal of Nuclear Materials, 1988. 155: p. 348-351.

78. Choi, S. and N. Bansal, *Mechanical behavior of zirconia/alumina composites.* Ceramics international, 2005. 31(1): p. 39-46.

79. Lakiza, S.M. and L.M. Lopato, *Stable and Metastable Phase Relations in the System Alumina–Zirconia–Yttria.* Journal of the American Ceramic Society, 1997. 80(4): p. 893-902.

80. Nieh, T.-G., J. Wadsworth, and O.D. Sherby, *Superplasticity in metals and ceramics*. 2005: Cambridge university press.

81. Rastogi, S. and G.E. Klingzing, *Characterizing the Rheology of Powders by studying dynamic avalanching of the powder.* Particle & Particle Systems Characterization, 1994. 11(6): p. 453-456.

82. Juste, E., et al., *Shaping of ceramic parts by selective laser melting of powder bed.* Journal of Materials Research, 2014. 29(17): p. 2086-2094.

83. Marcu, T., et al., *Effect of surface conditioning on the flowability of Ti6Al7Nb powder for selective laser melting applications.* Applied Surface Science, 2012. 258(7): p. 3276-3282.

84. Spierings, A.B., N. Herres, and G. Levy, *Influence of the particle size distribution on surface quality and mechanical properties in AM steel parts.* Rapid Prototyping Journal, 2011. 17(3): p. 195-202.

85. Sordelet, D.J. and M. Akinc, *Sintering of Monosized, Spherical Yttria Powders.* Journal of the American Ceramic Society, 1988. 71(12): p. 1148-1153.

86. Wilkes, J., et al., *Additive manufacturing of ZrO2 - Al2O3 ceramic components by selective laser melting.* Rapid Prototyping Journal, 2013. 19(1): p. 51-57.

87. Mapar, M., et al., *Preparation and flowability characterization of ceramic powders for Selective Laser Melting*, in *Advanced Research in Virtual and Rapid Prototyping* 2013: Leiria, Portugal.

88. Shah, R., M. Tawakkul, and M. Khan, *Comparative Evaluation of Flow for Pharmaceutical Powders and Granules.* AAPS PharmSciTech, 2008. 9(1): p. 250-258.

89. Zhang, Z. and M.F. Modest, *Temperature-Dependent Absorptances of Ceramics for Nd:YAG and CO2 Laser Processing Applications.* Journal of Heat Transfer, 1998. 120(2): p. 322-327.

90. Tolochko, N.K., et al., *Absorptance of powder materials suitable for laser sintering.* Rapid Prototyping Journal, 2000. 6(3): p. 155-161.

91. Exner, H., et al. *Selective laser micro sintering with a novel process*. 2003.

92. Fischer, P., et al., *A model for the interaction of near-infrared laser pulses with metal powders in selective laser sintering.* Applied Physics A, 2002. 74(4): p. 467-474.

93. Mumtaz, K.A., P. Erasenthiran, and N. Hopkinson, *High density selective laser melting of Waspaloy®.* Journal of Materials Processing Technology, 2008. 195(1–3): p. 77-87.

94. Gusarov, A.V. and I. Smurov, *Modeling the interaction of laser radiation with powder bed at selective laser melting.* Physics Procedia, 2010. 5, Part B(0): p. 381-394.

95. Gusarov, A.V., et al., *Model of Radiation and Heat Transfer in Laser-Powder Interaction Zone at Selective Laser Melting.* Journal of Heat Transfer, 2009. 131(7): p. 072101-072101.

96. Liu, F.R., et al., *Processing and characterizations of 2%PF/silica sand core–shell composite powders by selective laser sintering with a higher transmittance fiber laser.* International Journal of Machine Tools and Manufacture, 2012. 60(0): p. 52-58.

97. Streek, A., P. Regenfuss, and H. Exner, *Fundamentals of Energy Conversion and Dissipation in Powder Layers during Laser Micro Sintering.* Physics Procedia, 2013. 41(0): p. 858-869.

98. Gusarov, A.V. and J.P. Kruth, *Modelling of radiation transfer in metallic powders at laser treatment.* International Journal of Heat and Mass Transfer, 2005. 48(16): p. 3423-3434.

99. Kruth, J.P., et al., *Consolidation phenomena in laser and powder-bed based layered manufacturing.* CIRP Annals - Manufacturing Technology, 2007. 56(2): p. 730-759.

100. Vilaro, T., C. Colin, and J.D. Bartout, *As-Fabricated and Heat-Treated Microstructures of the Ti-6Al-4V Alloy Processed by Selective Laser Melting.* Metallurgical and Materials Transactions A, 2011. 42(10): p. 3190-3199.

101. Thomazin, J.A., L.G. Olson, and J.W. Hirsch, *Axisymmetric laser welding of ceramic and metallic materials: finite element modelling.* International Journal of Numerical Methods for Heat & Fluid Flow, 1996. 6(3): p. 35-46.

102. Yadroitsev, I. and I. Smurov, *Selective laser melting technology: From the single laser melted track stability to 3D parts of complex shape.* Physics Procedia, 2010. 5, Part B(0): p. 551-560.

103. Gu, D. and Y. Shen, *Balling phenomena in direct laser sintering of stainless steel powder: Metallurgical mechanisms and control methods.* Materials & Design, 2009. 30(8): p. 2903-2910.

104. Li, J.F., L. Li, and F.H. Stott, *Comparison of volumetric and surface heating sources in the modeling of laser melting of ceramic materials.* International Journal of Heat and Mass Transfer, 2004. 47(6–7): p. 1159-1174.

105. Yves-Christian, H., et al., *Net shaped high performance oxide ceramic parts by selective laser melting.* Physics Procedia, 2010. 5, Part B(0): p. 587-594.

106. Mercelis, P. and J.P. Kruth, *Residual stresses in selective laser sintering and selective laser melting.* Rapid Prototyping Journal, 2006. 12(5): p. 254-265.

107. D Munz, T.F., *Ceramics: mechanical properties, failure behaviour, materials selection* 1999.

108. Li, J.F., L. Li, and F.H. Stott, *Thermal stresses and their implication on cracking during laser melting of ceramic materials.* Acta Materialia, 2004. 52(14): p. 4385-4398.

109. Maehara, Y. and T. Langdon, *Superplasticity in ceramics.* Journal of Materials Science, 1990. 25(5): p. 2275-2286.

110. Fischer, P., et al., *Temperature measurements during selective laser sintering of titanium powder.* International Journal of Machine Tools and Manufacture, 2004. 44(12–13): p. 1293-1296.

Publications:

Journal Papers

1. C.Y. Yap, C.K. Chua, Z.H. Liu, D.Q. Zhang, L.E. Loh, S.L. Sing, M. Mapar & K.H. Low, *Review of Selective Laser Melting (2003 to 2013): Materials and Applications (Review Paper),* Journal of Materials processing Technology, 2014 (Submitted: 5-3-2014)

2. W. Y. Yeong, Z. Ziqiang, M. Mapar, P.C. Hung, L. Zhao, Z. Tian, B.Y. Tay & S. Yang , *Selective Laser Melting of Ceramics: A review* (To be submitted to Journal of the American Ceramic Society.)

Conference paper

1. M Mapar, DQ Zhang, ZH Liu, CK Chua, BY Tay, O Gramifard, S Maleksaeedi and FE Wiria , *Preparation and Flowability Characterization of Ceramic Powders for Selective Laser Melting,* International Conference in Advanced Research in Virtual and Rapid Prototyping, VRAP, Leiria, Portugal, 1 – 5 Oct 2013.
2. WY Yeong, CY Yap, M Mapar and CK Chua, *State-of-the-Art Review on Selective Laser Melting of Ceramics,* International Conference in Advanced Research in Virtual and Rapid Prototyping, VRAP, Leiria, Portugal, 1 – 5 Oct 2013.
3. M. Mapar, W. Y. Yeong, B.Y. Tay, F.E. Wiria and C.K. Chua, *Flow Behaviour Investigation of Al_2O_3-ZrO_2 Ceramic Powder for Selective Laser*

Melting Technique, International Conference on Progress in Additive Manufacturing, Pro-AM, Singapore.26-28 May 2014.

4. Z. Zhao, M. Mapar, W. Y. Yeong, S. Zhang & D. Zhao ,*Experiment Investigation on Selective Laser Melting of ZrO_2/Al_2O_3 Ceramics*, International Conference on Progress in Additive Manufacturing, Pro-AM, Singapore. 26-28 May 2014.